

FINITE ELEMENT ANALYSES OF DIFFERENTIAL SHRINKAGE-INDUCED  
CRACKING IN CENTRIFUGALLY CAST CONCRETE POLES

A THESIS SUBMITTED TO  
THE GRADUATE SCHOOL OF NATURAL AND APPLIED SCIENCES  
OF  
MIDDLE EAST TECHNICAL UNIVERSITY

BY

TUĞRUL TANFENER

IN PARTIAL FULFILLMENT OF THE REQUIREMENTS  
FOR  
THE DEGREE OF MASTER OF SCIENCE  
IN  
CIVIL ENGINEERING

SEPTEMBER 2012

Approval of the thesis:

**FINITE ELEMENT ANALYSES OF DIFFERENTIAL  
SHRINKAGE-INDUCED CRACKING IN CENTRIFUGALLY CAST CONCRETE POLES**

submitted by **TUĞRUL TANFENER** in partial fulfillment of the requirements for the degree of **Master of Science in Civil Engineering Department, Middle East Technical University** by,

Prof. Dr. Canan Özgen  
Dean, Graduate School of **Natural and Applied Sciences**

\_\_\_\_\_

Prof. Dr. Güney Özcebe  
Head of Department, **Civil Engineering**

\_\_\_\_\_

Asst. Prof. Dr.Serdar Göktepe  
Supervisor, **Civil Engineering Dept., METU**

\_\_\_\_\_

Prof. Dr. İsmail Özgür Yaman  
Co-supervisor, **Civil Engineering Dept., METU**

\_\_\_\_\_

**Examining Committee Members:**

Prof. Dr. Barış Binici  
Civil Engineering Dept., METU

\_\_\_\_\_

Asst. Prof. Dr. Serdar Göktepe  
Civil Engineering Dept., METU

\_\_\_\_\_

Prof. Dr. İsmail Özgür Yaman  
Civil Engineering Dept., METU

\_\_\_\_\_

Assoc. Prof. Dr. Afşin Sarıtaş  
Civil Engineering Dept., METU

\_\_\_\_\_

Asst. Prof. Dr. Ercan Gürses  
Aerospace Engineering Dept., METU

\_\_\_\_\_

**Date: 06.09.2012**

**I hereby declare that all information in this document has been obtained and presented in accordance with academic rules and ethical conduct. I also declare that, as required by these rules and conduct, I have fully cited and referenced all material and results that are not original to this work.**

Name, Last Name: TUĞRUL TANFENER

Signature:

## **ABSTRACT**

### **FINITE ELEMENT ANALYSES OF DIFFERENTIAL SHRINKAGE-INDUCED CRACKING IN CENTRIFUGALLY CAST CONCRETE POLES**

Tanfener, Tuğrul

M.Sc., Department of Civil Engineering

Supervisor: Asst. Prof. Dr. Serdar Göktepe

Co-Supervisor: Prof. Dr. İsmail Özgür Yaman

September 2012, 68 pages

Poles are used as an important constituent of transmission, distribution and communication structures; highway and street lighting systems and other various structural applications. Concrete is the main production material of the pole industry. Concrete is preferred to steel and wood due not only to environmental and economic reasons but also because of its high durability to environmental effects and relatively less frequent maintenance requirements.

Centrifugal casting is the most preferred way of manufacturing concrete poles. However, misapplication of the method may lead to a significant reduction in strength and durability of the poles. Segregation of concrete mixture is a frequent problem of centrifugal casting. The segregated concrete within the pole cross-section possesses different physical properties. In particular, the shrinkage tendency of the inner concrete, where the cement paste is accumulated, becomes significantly larger. Differential shrinkage of hardened concrete across the pole section gives rise to the development of internal tensile stresses, which, in turn, results in longitudinal cracking along the poles.

There is a vast literature on experimental studies of parameters affecting differential shrinkage of centrifugally cast poles. This research aims to computationally investigate the differential shrinkage-induced internal stress development and cracking of concrete poles. To this end, two and three-dimensional mathematical models of the poles are constructed and

finite element analyses of these models are carried out for different scenarios. The computationally obtained results that favorably agree with the existing experimental data open the possibility to improve the centrifugal manufacturing technique by using computational tools.

Keywords: Concrete poles, centrifugal casting, spun-cast, differential shrinkage, finite element modeling

## ÖZ

### **MERKEZKAÇ DÖKÜMLÜ BETON DİREKLERDE OLUŞAN RÖTRE ÇATLAKLARININ SONLU ELEMANLAR YÖNTEMİ KULLANILARAK İNCELENMESİ**

Tanfener, Tuğrul

Yüksek Lisans, İnşaat Mühendisliği Bölümü

Tez Yöneticisi : Yrd. Doç. Dr. Serdar Göktepe

Ortak Tez Yöneticisi : Prof. Dr. İsmail Özgür Yaman

Eylül 2012, 68 sayfa

Aydınlatma, elektrik dağıtımı, iletişim ağları ve benzeri pek çok alanda direkler kullanılmaktadır. Günümüzde direklerin imalatında kullanılan en ekonomik ve elverişli malzeme olan beton, ahşap ve metale kıyasla daha ekonomik, uzun süre bakım gerektirmeyen dayanıklı bir malzemedir. Betonarme direklerin imalatında çoğunlukla merkezkaç döküm yöntemi kullanılmaktadır. Bu yöntemin kullanımı ile içi boş tüp şeklinde imal edilen direklerin, dolu gövdeli direklere göre pek çok yönden üstünlüğü bulunmaktadır. Direk içerisinde oluşan boşluk ağırlığı azaltmakla birlikte çeşitli iletim kablolarının geçişine de olanak vermektedir.

Merkezkaç döküm, betonarme direklerin üretiminde oldukça iyi bir teknik olmakla birlikte üretim aşamasında yapılabilecek hatalar direklerin dayanım ve dayanıklılığını önemli ölçüde azaltabilmektedir. Bu teknikte karşılaşılan yaygın sorunlardan biri de döküm sonrası kalıbın döndürülmesi esnasında kesitte meydana gelen ayrışmadır. Ayrışma, direğin iç ve dış yüzeylerinde farklı özelliklere sahip beton karışımlarının oluşmasına sebep olmakta, farklı özelliklere sahip karışımların aynı zamanda farklı rötre özelliklerine sahip olması nedeniyle beton direk boyunca çatlaklar meydana gelebilmektedir. Betonun çatlaması, elemanın pek çok çevresel etkene karşı direncini, dolayısıyla kullanım ömrünü azaltmaktadır.

Üretilen elemanların farklı rötre etkilerine maruz kalmaması için üretim aşamasında hazırlanan beton karışımı, katkı maddeleri, kalıbın döndürülme hızı ve süresi gibi parametrelere dikkat edilmelidir. Bu parametrelerin merkezkaç dökümlü elemanlar üzerindeki

etkisini arařtıran laboratuvar alıřmaları literatürde mevcuttur. Bu alıřmanın amacı, literatürdeki deneysel verileri kullanarak, merkezka dökümlü beton direklerin farklı rötre etkisi altındaki davranıřlarını sonlu elemanlar yöntemi kullanarak incelemektir. Yapılan modellemelerden elde edilen sonuca göre bu tür ayrıřmalar beton direklerin iç kısımlarında atlakların oluřtuđunu ve bu atlakların dıřarıya doğru ilerlediđini göstermiřtir.

Anahtar Kelimeler: Merkezka döküm, farklı rötre, beton direk, rötre atlakları, sonlu elemanlar yöntemi

## **ACKNOWLEDGEMENTS**

I would like to express my sincere gratitude to my advisor Asst. Prof. Dr. Serdar Göktepe and my co-advisor Prof. Dr. İsmail Özgür Yaman for their continuous support, guidance and motivation throughout the study.

I would also like to thank to the faculty members in Construction Materials and Structural Engineering Divisions who contributed to my graduate education.

Finally, I wish to thank my family including my parents, brother and fiancée for their patience and support during the study.



## TABLE OF CONTENTS

ABSTRACT .....	iv
ÖZ .....	vi
ACKNOWLEDGEMENTS .....	viii
TABLE OF CONTENTS .....	ix
LIST OF TABLES.....	xi
LIST OF FIGURES.....	xii
1. INTRODUCTION.....	1
1.1 Concrete Poles.....	1
1.2 Motivation of the Study .....	1
1.3 Outline .....	2
2. LITERATURE REVIEW .....	4
2.1 Production of Concrete Poles with Centrifugal Casting Method .....	4
2.2 Durability Problems Encountered on Concrete Poles .....	6
2.3 Properties of Materials and Specimens Used in the Experimental Studies.....	7
2.4 Segregation of Concrete during Centrifugal Casting .....	8
2.5 Drying Shrinkage .....	11
2.6 Differential Shrinkage .....	11
3. XFEM CRACK MODELING FOR FRACTURE OF CONCRETE .....	15
3.1 Fracture Mechanics for Concrete.....	15
3.1.1 Characteristic Fracture Properties of Concrete .....	18
3.2 Introduction to Fracture Mechanics of Brittle Materials .....	20
3.2.1 Linear Elastic Fracture Mechanics (LEFM).....	21
3.2.2 Nonlinear Fracture Mechanics (NLFM).....	27
3.3 Crack modeling Techniques for Concrete Fracture.....	31
3.3.1 Local and Non-Local Models for Crack Propagation Analysis .....	31
3.3.2 Smeared Crack Model.....	32
3.3.3 Discrete Interface Crack Model .....	32
3.3.4 Discrete Cracked-Element Model.....	33
3.3.5 Enriched Elements and Other Techniques .....	33
3.4 The Extended Finite Element Method (XFEM) .....	34

3.4.1	XFEM Formulation .....	35
3.4.2	Cohesive Crack Growth with XFEM .....	36
3.4.3	The Level Set Method .....	37
3.4.4	Crack Propagation Analysis Example with XFEM in ABAQUS .....	39
4.	NUMERICAL MODELING AND ANALYSES.....	44
4.1	Two-Dimensional Analyses .....	44
4.1.1	Plane-Strain Assumption .....	45
4.1.2	Model Geometry.....	45
4.1.3	Designation of the Boundary Conditions .....	46
4.1.4	Material Properties .....	47
4.1.5	Loading Conditions.....	48
4.2	Two-Dimensional Stress Analyses Results.....	49
4.2.1	Development of Stresses .....	49
4.2.2	Interpretation of the Analyses Results .....	52
4.3	Two-Dimensional Crack Propagation Analysis .....	54
4.3.1	Crack Initiation Criterion .....	54
4.3.2	Crack Propagation Criterion .....	54
4.4	Results of the Two-Dimensional Crack Propagation Analysis.....	57
4.5	Multiple Crack Formation.....	59
4.6	Effect of Reinforcement .....	60
4.7	Three-Dimensional Analyses .....	61
4.7.1	Model Geometry and Properties .....	61
4.8	Results of the Three-Dimensional Stress Analysis.....	62
4.9	Results of the Three-Dimensional Crack Propagation Analysis .....	62
4.10	Discussion on Limitations of the Study.....	63
5.	CONCLUSION.....	65
	REFERENCES.....	67

## **LIST OF TABLES**

### **TABLES**

Table 1: Concrete mix proportions (Dilger, Ghali and Rao 1996) .....	7
Table 2: Appropriate Theories for Analyzing Failure (Bazant 2002) .....	18
Table 3: Elastic material properties.....	48
Table 4: Summary of the results .....	53

## LIST OF FIGURES

### FIGURES

Figure 1: Concrete poles (AFG-EL 2012).....	2
Figure 2: Centrifugal casting method (Rodgers 1984) (Kudzys and Kliukas 2008) .....	5
Figure 3: (a) Vertical cracking and spalling, (b) Freeze and thaw damage .....	7
Figure 4: Pole specimen dimensions and reinforcement arrangement.....	9
Figure 5: Segregated pole section (Dilger, Ghali and Rao 1996) .....	9
Figure 6: Distribution profile of the damaged pole (Dilger, Ghali and Rao 1996).....	10
Figure 7: Distribution profile of the pole specimen (Dilger, Ghali and Rao 1996) .....	10
Figure 8: Drying shrinkage induced stress development (Mehta and Monteiro 2006).....	12
Figure 9: Differential shrinkage of bamboo flutes (NavaChing 2008).....	12
Figure 10: Shrinkage in separate layers of pole wall (Dilger, Ghali and Rao 1996) .....	13
Figure 11: Free shrinkage across wall thickness after 63 Days (Dilger, Ghali and Rao 1996). .....	14
Figure 12: Typical crack pattern in laboratory specimens (Dilger, Ghali and Rao 1996).....	14
Figure 13: Different categories of continuities (Mohammadi 2008).....	16
Figure 14: Spurious mesh sensitivity (ACI Committee 446 1991) .....	17
Figure 15: Load-deflection diagram of ductile and brittle structures (ACI Committee 446 1991) .....	18
Figure 16: (a) Typical tensile load-deformation response and (b) illustration of the fracture process zone of concrete (Asferg 2006).....	19
Figure 17: Linear zone (L), nonlinear zone (N) and fracture process zone (F) in fracture of different materials (ACI Committee 446 1991) .....	20
Figure 18: An infinite plate with a central crack subjected to tension (left), and subjected to shear (right) (Shi 2009) .....	23
Figure 19: Modes of deformation at the crack-tip .....	25
Figure 20: (a) Dugdale cohesive model, (b) Barenblatt cohesive model (Shi 2009).....	29
Figure 21: Illustration of the fictitious crack model (Asferg 2006).....	29
Figure 22: Development phases of FPZ (Shi 2009) .....	30
Figure 23: Load-deformation curve and tension softening curve (Shi 2009) .....	30
Figure 24: CBM stress-strain curve for crack propagation (Asferg 2006) .....	31
Figure 25: Illustration of a smeared crack (Mohammadi 2008).....	32

Figure 26: (a) Discrete cracked element (b) Enriched element: crack can propagate through the elements regardless of the mesh geometry (Mohammadi 2008) .....	34
Figure 27: Regions of a crack for enrichment (Dolbow , Moës and Belytschko 2000).....	36
Figure 28: Illustration of normal and tangential coordinates for a smooth crack (ABAQUS 6.10 2010). .....	36
Figure 29: Domain with a crack involving cohesive zone (Moës and Belytschko 2002) .....	37
Figure 30: Definition of the level set function (Mohammadi 2008).....	38
Figure 31: Representation of a non-planar crack in three-dimensions by two level set functions (ABAQUS 6.10 2010).....	38
Figure 32: Geometry of the benchmark problem (Mohammadi 2008) .....	39
Figure 33: The expected crack propagation pattern (Mohammadi 2008).....	40
Figure 34: Loading / boundary conditions and mesh geometry of the XFEM model.....	40
Figure 35: Crack propagation pattern of the XFEM analysis with level set contours.....	41
Figure 36: Loading / boundary conditions and mesh geometry of the XFEM model.....	41
Figure 37: Crack propagation pattern of the four-point bending beam example .....	42
Figure 38: Load-displacement curve of four-point bending beam example.....	42
Figure 39: Load-displacement curve of four-point bending beam example from textbook by Mohammadi (Mohammadi 2008).....	43
Figure 40: Plane-strain assumption for two-dimensional pole models .....	45
Figure 41: Selection of the element type in ABAQUS.....	46
Figure 42: Discretization of the member.....	46
Figure 43: (a) 2D model dimensions, (b) Boundary conditions .....	47
Figure 44: (a) Nonlinear distribution of experimental shrinkage measurements (Dilger and Rao 1997), (b) Parabolic shrinkage distribution curve .....	48
Figure 45: Analyses cases with increasing shrinkage gradient .....	49
Figure 46: Maximum in-plane principal stress diagrams – Case 1 .....	50
Figure 47: Maximum in-plane principal stress diagrams – Case 2 .....	51
Figure 48: Maximum in-Plane principal stress diagrams – Case 3 .....	52
Figure 49: Maximum in-plane principal stress diagrams – Case 4 .....	53
Figure 50: Setting the damage initiation criterion .....	55
Figure 51: The softening curve of concrete.....	56
Figure 52: Setting the crack propagation criterion .....	56
Figure 53: Imperfection for the crack initiation.....	57
Figure 54 Stages of the crack propagation .....	58
Figure 55: Simultaneous multiple crack formation .....	59
Figure 56: Crack propagation in reinforced cross-section .....	60

Figure 57: Three-dimensional analysis model .....	61
Figure 58: Maximum principal stress diagrams – Case 1.....	62
Figure 59: Maximum principal stress diagrams – Case 2.....	63
Figure 60: Level set contours of three-dimensional crack propagation.....	64

# **CHAPTER I**

## **INTRODUCTION**

### **1.1 Concrete Poles**

Poles are widely used as an important constituent of transmission, distribution and communication structures; highway and street lighting systems and other various structural applications where piers are needed (Figure 1). Through long ages, the conventional material for manufacturing poles was wood; however, environmental concerns created the need for a new material for the pole industry. Steel poles constitute a good alternative for poles in terms of having sufficient strength properties with lighter sections. But, high cost of steel production and the requirement of the continuous protection against corrosion make concrete poles more beneficial. Therefore, concrete has been substituted for wood as the main production material of the pole industry. Concrete is preferred to steel and wood due not only to environmental and economic reasons but also because of its high durability to environmental effects and relatively less frequent maintenance requirements.

### **1.2 Motivation and Objective of the Study**

Concrete poles are needed to be designed by considering various loading conditions such as wind and seismic loads. Therefore, pre-stressed or regular reinforcements are usually used to provide sufficient flexural capacity. In that case, corrosion of steel reinforcement turns into a major durability problem for the concrete poles. Since a transmission, distribution or lighting system contains a vast number of poles, it is crucial to avoid such durability problems which would bring a lot of maintenance costs.

The most preferred production method of concrete poles is the centrifugal casting. By use of this method, hollow sections of concrete poles are produced. The reduced weight of hollow poles creates the advantage of easier transportation which demands less cost. Moreover, a high quality concrete can be manufactured, since the centrifugal casting method has a better capability of compaction. Despite these advantageous properties, severe durability problems can occur if the method is not applied properly and leads to the segregation of

concrete. The centrifugally-cast concrete poles, which have segregated cross-sections, undergo longitudinal cracking due to differential shrinkage and become prone to severe durability problems.

This study aims to investigate the abovementioned unique problem by using computational techniques. In this regard, two and three-dimensional finite element analyses are performed based on experimental data provided by several researchers. The intention is to provide quantitative results that support the experimental observations in the literature, and so contribute to the solution of the problem.

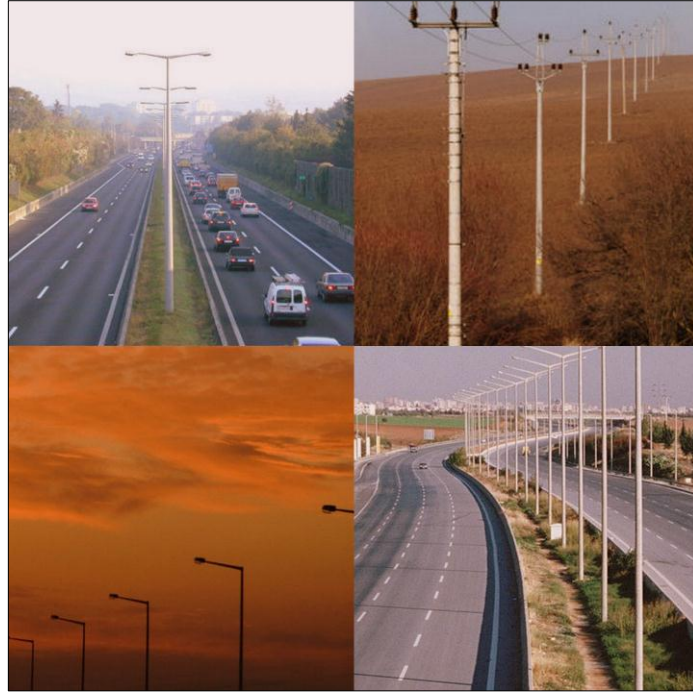


Figure 1: Concrete poles (AFG-EL 2012)

### 1.3 Outline

Since this study is based on the experimental data provided in the literature, broad information about these data is given in Chapter 2. In Chapter 2, details of the production technique and brief theoretical knowledge about the encountered problem are presented.

Chapter 3 aims to provide fundamental principles of fracture mechanics theories. Especially the failure characteristics of concrete are explained in detail. Moreover, in this chapter, the extended finite element method for crack propagation analyses is introduced.



In Chapter 4, the performed computational analyses within this thesis are presented. Chapter 4 contains the results of two and three-dimensional finite element analyses and the comparison of the results with the source experimental data. Furthermore, the initiation of cracking, crack propagation pattern and the extent of the failure zone are shown in Chapter 4.

Finally, some concluding remarks and outlook are outlined in Chapter 5.

## **CHAPTER II**

### **LITERATURE REVIEW**

The review of literature is presented in this chapter to give the fundamental background about the experimental studies on differential shrinkage-induced cracking of concrete poles. Quantitative results of these experiments are explained comprehensively, since these results constitute the source data for computer modeling. Moreover, literature on main components of the problem; such as the production method, segregation of concrete and differential shrinkage, is also introduced as part of the literature review.

The literature search has shown that a considerable amount of experimental studies about the subject is present. However, computer modeling based computational studies; particularly analyzing the differential shrinkage-induced cracking, are very rare. This is the reason why there is no computational research mentioned throughout this chapter.

#### **2.1 Production of Concrete Poles with Centrifugal Casting Method**

Since the problem is originated because of misapplications made during the production phase; the method of manufacturing is introduced at the outset. There are two main methods commonly used in concrete pole production. First one is static casting and the other one is centrifugal casting (also known as spin casting). The static casting method is performed by conventional practices of concrete member production by using regular formwork and vibration process for compaction. The centrifugal casting, on the other hand, is a special technique for casting concrete poles which requires form spinning equipment for the compaction of concrete and is generally preferred to the static casting method due to its several advantages (PCI 1997).

In brief, centrifugal casting is performed by forms having two separable halves with spinning ring equipment (Figure 2). A prescribed amount of concrete is pumped into the horizontally placed lower half of the form, following the installation of reinforcements. The lower and upper parts are assembled together with bolts, after that, wheels of the machine spin the form at a specified speed for a specified duration. Centrifugal forces provide the desired

compaction by compressing concrete to the form surface. In this way, well-compacted spun-cast concrete poles are produced with a central void. The central void of spun-cast poles provides the benefits of reducing the weight of concrete poles, and thus the transportation and installation costs. It also allows a passage of cables or other required installation through the poles. Centrifugal casting becomes superior to static casting by eliminating the need of extra formwork for the central void. In addition to the advantages related with the central void, well produced spun-cast poles have better compaction with a dry unit weight of 2483 to 2643 kg/m<sup>3</sup>, while that of statically-cast poles ranges from 2323 to 2403 kg/m<sup>3</sup>. Besides, spun-cast poles have an improved bond between steel reinforcement and concrete, also a smoother surface finish (PCI 1997).

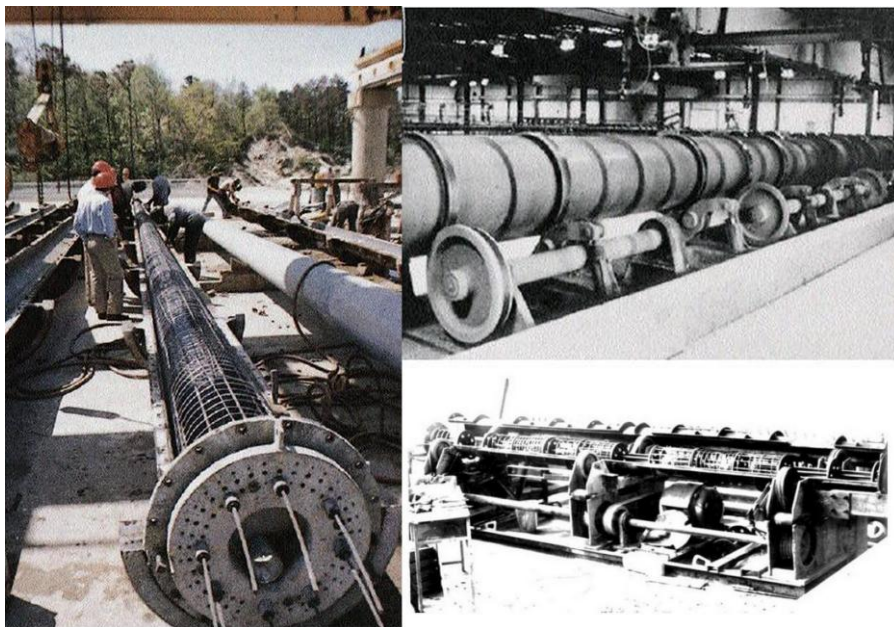


Figure 2: Centrifugal casting method (Rodgers 1984) (Kudzys and Kliukas 2008)

Although centrifugal casting is the most preferred way of manufacturing concrete poles, improper applications of spinning process or inadequately designed concrete mixtures may lead to segregation of the constituents of concrete and thus serious durability problems. There are some precautions which should be taken in order to minimize segregation of constituents. One of them is having a proper design of concrete mixture and the other one is adjusting the spinning rate and duration appropriately.

Concrete mixture needs to be designed to have a consistency which holds constituents together, also an adequate workability when forms are spun. The duration and rate of spinning must be high enough to provide satisfactory compaction, and must be limited in order to prevent segregation as well (Dilger, Ghali and Rao 1996).

## **2.2 Durability Problems Encountered on Concrete Poles**

Durability problems of poles usually arise from the existing cracks in concrete. If pole structures are exposed to open air conditions, then water can penetrate concrete section through cracks and initiate detrimental reactions inside concrete, or directly cause damage by freezing and thawing cycles.

According to the site surveys conducted by utility companies on approximately a hundred damaged poles in Eastern Canada, one of the most encountered problems was freezing and thawing cycle damages in the absence of adequate frost resistance. The other frequently observed type of damage was the extensive vertical cracking of concrete poles (Figure 3), where the cracks varied from 0.05mm to 12mm in width. A comprehensive laboratory investigation of a damaged pole by the researchers showed that vertical cracking initiates at the inside surface of the pole and propagates towards the outside layers. It is clear that cracks leaved the concrete poles vulnerable to environmental effects when reached to the outside surface (Dilger, Ghali and Rao 1996).

Earlier assumptions stated that the longitudinal cracking of concrete occurs because of different drying conditions or differential temperature variation inside and outside of the poles. Another assumption indicated that freezing of water inside the pole would cause the excessive tensile stresses thus cracking. Researchers investigated the reasons of longitudinal cracking of concrete poles by inspecting the abovementioned old damaged pole in laboratory and further conducting a series of experiments with long term measurements on prepared specimens. Their experimental studies revealed that if the concrete mixture was not designed properly or the production technique was inappropriately applied, then segregation of constituents of the concrete mixture occurred throughout the cross-section. The causes and effects of segregation will be discussed in detail in the following parts (Dilger, Ghali and Rao 1996).

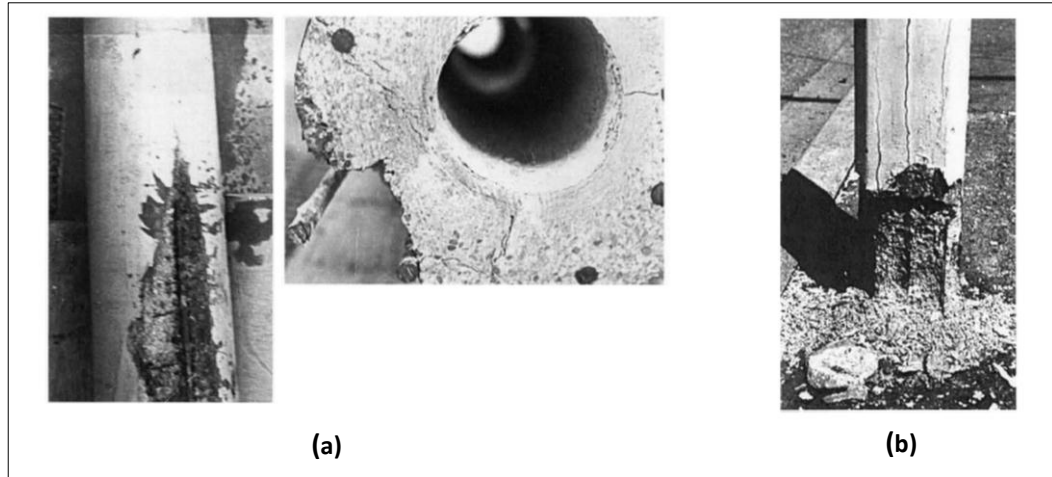


Figure 3: (a) Vertical cracking and spalling, (b) Freeze and thaw damage (Dilger, Ghali and Rao 1996)

### 2.3 Properties of Materials and Specimens Used in the Experimental Studies

The data used in computational modeling are mainly obtained from the experimental studies of Dilger et al (Dilger, Ghali and Rao 1996). These experimental studies consist of two main parts; the first part was the examination of causes of the observed damage and the second part was a parametric study for developing a suitable mix. The analyses of this study are based on the measurements presented by researchers in the first part. Within the scope of the first part; subsequent to the investigation of the damaged pole, a laboratory specimen was produced to simulate a similar damage (Dilger, Ghali and Rao 1996).

Table 1: Concrete mix proportions (Dilger, Ghali and Rao 1996)

Cement	507 kg/m <sup>3</sup>
Water	193 kg/m <sup>3</sup>
Sand	611 kg/m <sup>3</sup>
Gravel	1129 kg/m <sup>3</sup>
Water-Cement Ratio	0.38
<i>Admixtures</i>	
Water-Reducing Agent	0.430 liter/100 kg of cement
Air-Entraining Agent	0.125 liter/100 kg of cement
Sand-to-Gravel Ratio	0.35/0.65

Laboratory specimen was produced by spin-casting at a rate of 300 revolutions per minute for 10 minutes. The concrete mixtures were prepared by using proportions given in Table 1, had a 5 cm slump and 4% to 5% air entrainment. The purpose of using air-entrained concrete was to eliminate frost damage and focus solely on the differential shrinkage-induced cracking. The pole was 12 m long and composed of eight segments which had different reinforcement arrangements (Figure 4). The longest segment (segment 4) was intended to be used for bending test, and the rest were assigned for shrinkage tests. After the casting process had been completed, concrete members have been reserved at approximately 60°C for 7 hours. Three of seven segments were kept in laboratory at 20°C temperature and 40% relative humidity, and the other four segments were kept in the open air. A piece was cut from the longest segment and further sliced into pieces with the purpose of measuring shrinkage strains of the different layers through the pole section. These pieces were kept in laboratory conditions and were tested periodically for 18 months (Dilger, Ghali and Rao 1996).

## **2.4 Segregation of Concrete during Centrifugal Casting**

A typical concrete mixture contains particles of different sizes. Aggregate sizes of the mixtures used in the experimental studies varied between approximately 160µm to 20mm in diameter (Dilger and Rao 1997). The particles of various sizes also have different masses; accordingly, constituents are affected differently from the centrifugal forces generated by spinning of the forms. The coarse aggregates with bigger masses are the most affected, and tend to move towards the outer part of concrete section. Similarly, cement and other cementitious materials, the finest constituents, affected less, thus tend to accumulate in the inner part of cross-section (Figure 5) (Dilger, Ghali and Rao 1996).

The provided grain-size distributions clearly show the extent of segregation across the cross-section of concrete poles. For the investigated old damaged pole, 55% of the inner segment is composed of hydrated cement paste while the amount of cement decreases to 20% in the outer part of the cross-section (Figure 6). Similarly for the newly produced pole specimen, it was observed that 50% of the inner part and 15% to 20% of the outer part comprised cement paste (Figure 7). Another observation was the accumulation of the entrained air in the inner surface, which also indicated the less effect of centrifugal forces on lighter constituents (Dilger, Ghali and Rao 1996).

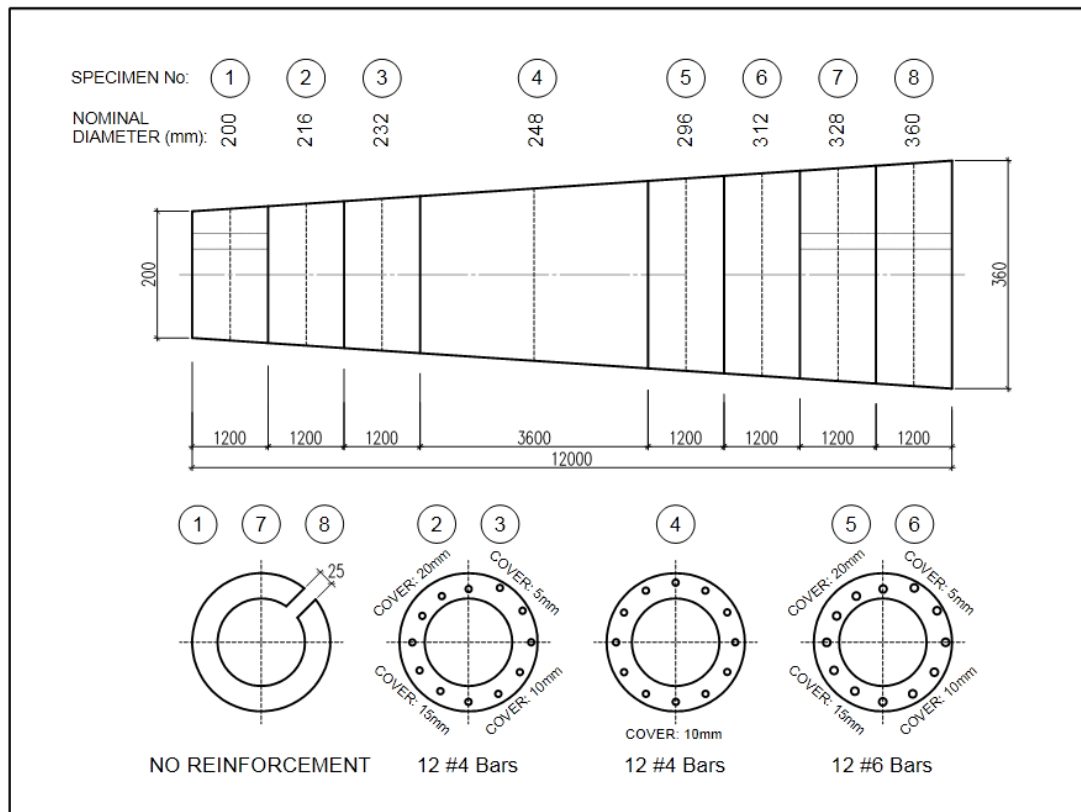


Figure 4: Pole specimen dimensions and reinforcement arrangement (Dilger, Ghali and Rao 1996)

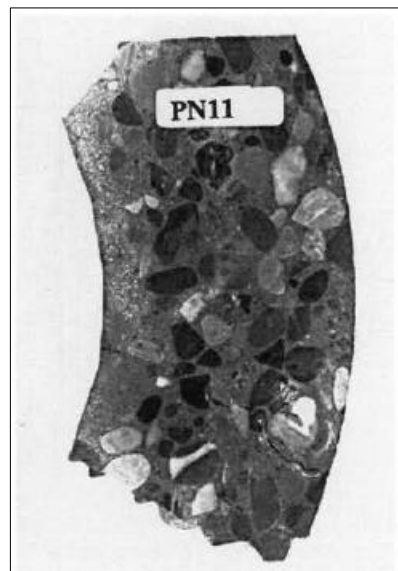


Figure 5: Segregated pole section (Dilger, Ghali and Rao 1996)

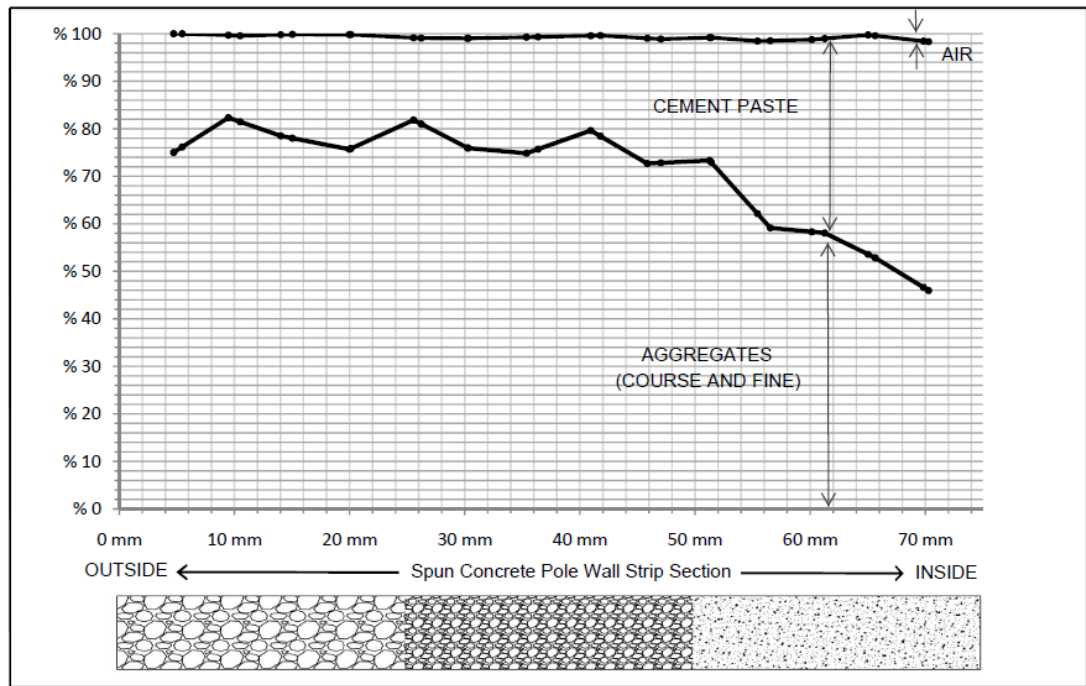


Figure 6: Distribution profile of the damaged pole (Dilger, Ghali and Rao 1996)

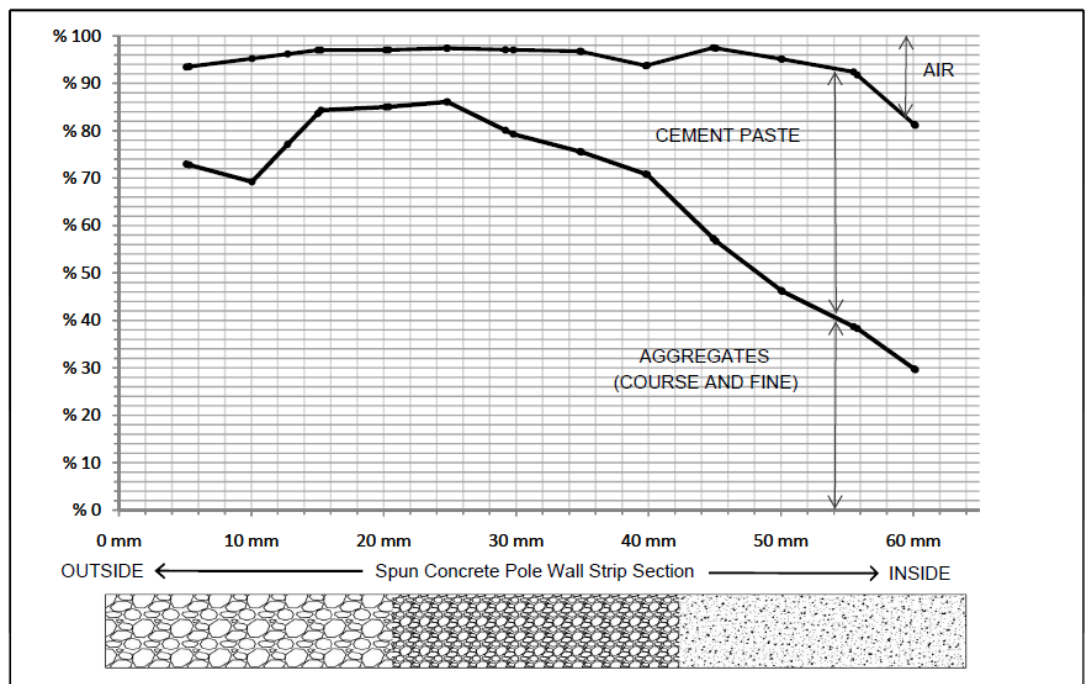


Figure 7: Distribution profile of the pole specimen (Dilger, Ghali and Rao 1996)



The researchers suggested that the poles with segregated sections are the ones which suffer from the vertical cracking problem. It was concluded that segregation of the concrete section leads to a phenomenon called differential shrinkage; which results in growth of the excessive tensile stresses, and as a result the longitudinal cracking of concrete pole sections. Differential shrinkage will be thoroughly explained in the following parts (Dilger, Ghali and Rao 1996).

## **2.5 Drying Shrinkage**

The microstructure of concrete is capable of containing water inside by means of the voids. The water held inside relatively larger voids ( $>50\text{nm}$ ) is called the free water, and removal of which does not cause any contraction. However, the loss of water in smaller capillaries ( $5\text{nm}$  to  $50\text{nm}$ ), or loss of the interlayer water held by C-S-H structure causes drying shrinkage of concrete. Drying shrinkage occurs when the ambient relative humidity is below saturation; in other words, when it is less than 100%. As the concrete microstructure dries, the hydrostatic pressure provided by the water is lost. Therefore, solid walls of the capillary pores, which are supported by the hydrostatic pressure, are subjected to compressive stresses leading to the contraction of the whole structure. A concrete member would dry and contract if it is exposed to low humidity. But, in case the member is restrained, development of shrinkage strains will be prevented and tensile stresses will generate instead of contraction. And consequently the tensile stresses cause cracking of concrete (Mehta and Monteiro 2006).

## **2.6 Differential Shrinkage**

Concrete is not the only material which suffers from adverse effects of shrinkage, but almost all brittle materials are affected similarly. As an example, flutes made of bamboo can undergo cracking when they are subjected to drying (Figure 9). Apparently, the flutes are not restrained and free to contract without any tensile stresses developed. So normally no cracking is expected due to shrinkage; however, if the outside and inside surfaces of the flute lose different amounts of moisture, then these surfaces would have uneven shrinkage strains. Inhomogeneous distribution of strains over the cross-section generates tensile stresses concentrated in the more contracted surface (NavaChing 2008). The abovementioned type of shrinkage is called differential shrinkage.

It was stated in the preceding section that drying shrinkage is caused by the water loss from hydrated cement paste. In case of the spun-cast concrete poles, cement paste accumulates in the inner part of pole section due to segregation. As a consequence, shrinkage strains become higher in the inner circumference and tensile stresses develop throughout the cross-section because of differential shrinkage.

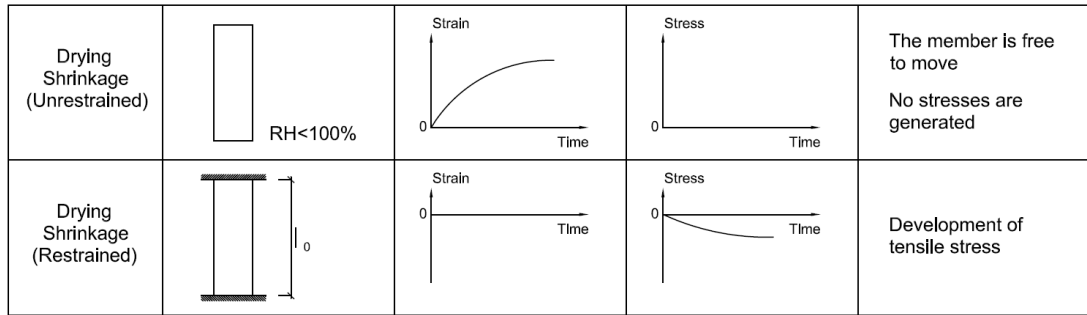


Figure 8: Drying shrinkage induced stress development (Mehta and Monteiro 2006)

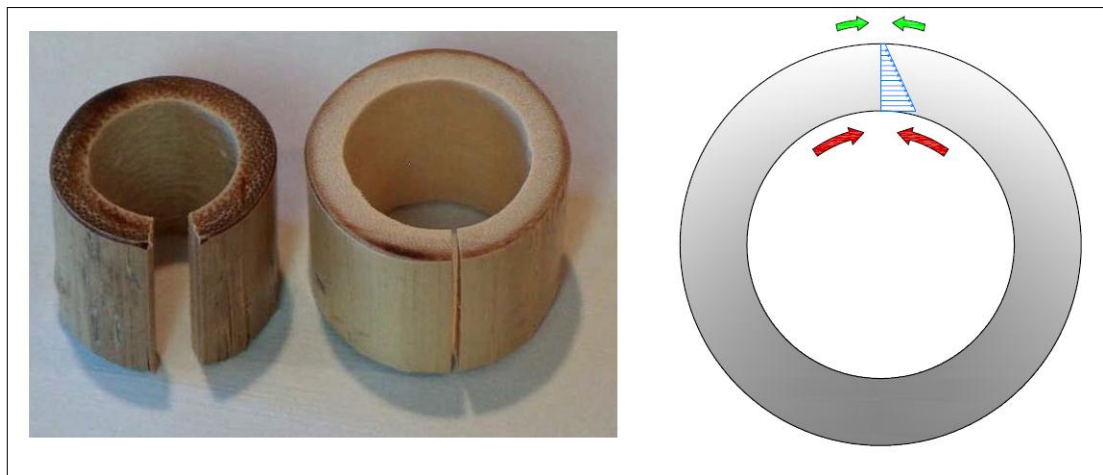


Figure 9: Differential shrinkage of bamboo flutes (NavaChing 2008)

The researchers confirmed differential shrinkage behavior of the pole specimen by using two different methods. The first method was to form a continuous slot along of the pole cross-section (Figure 4); closure of the slot was intended to point out the higher shrinkage of the inner circumference, and unchanged width of the slot to point out the uniform shrinkage. Three unreinforced segments of the pole specimen were produced with a 25 mm width longitudinal slot. Accordingly, the slots on the pole segments, which were kept in laboratory conditions for 9 months, closed by 2.4 mm thus indicated differential shrinkage of inner and outer layers. The second and more precise method of confirmation of differential shrinkage was the strain monitoring of concrete slices cut from different layers of the pole section. Concrete slices were stored in relatively dry conditions while their shrinkage strains were measured. The presented measurements showed that the shrinkage strains of the inner layer exceeded approximately 10 times the shrinkage strains measured in the outer layer

(Figure 10), the researchers plotted the values of free shrinkage to indicate the nonlinear shrinkage variation of the cross-section (Figure 11) (Dilger, Ghali and Rao 1996).

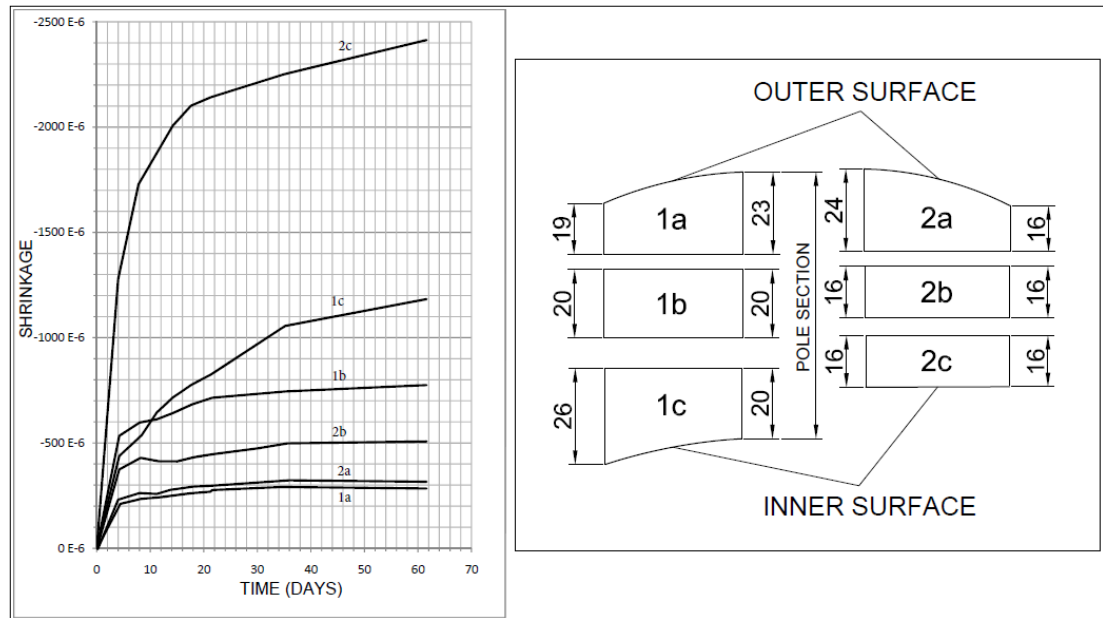


Figure 10: Shrinkage in separate layers of pole wall (Dilger, Ghali and Rao 1996)

The researchers reported that the differential shrinkage-induced vertical cracking initiated from the inner surface of the pole specimen (Figure 12). Therefore, the assumptions regarding the concentration of tensile stresses at the inner layers, where cement paste was accumulated, were confirmed. It was also observed that, propagation of cracking towards outer layers stopped where cracks confronted by rebar or larger aggregates (Dilger, Ghali and Rao 1996).

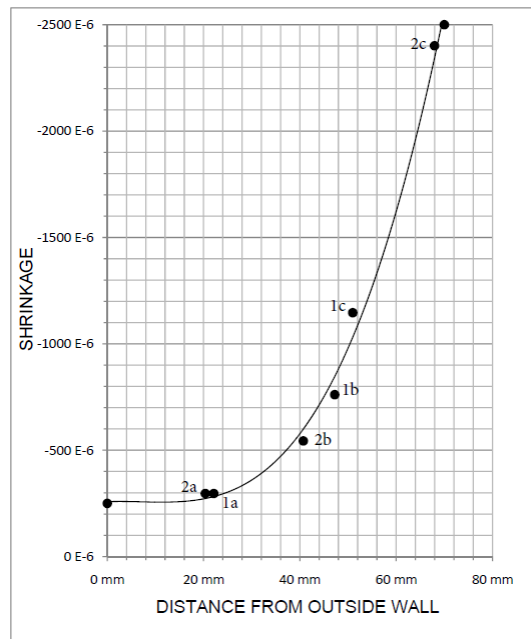


Figure 11: Free shrinkage across wall thickness after 63 Days (Dilger, Ghali and Rao 1996).

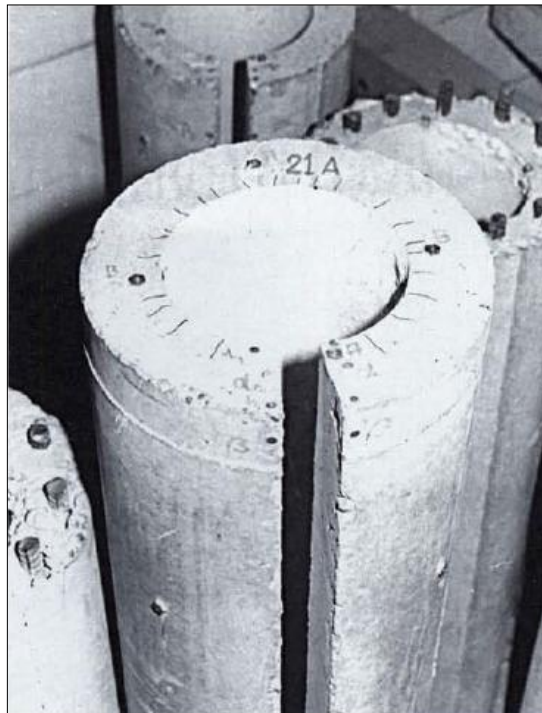


Figure 12: Typical crack pattern in laboratory specimens (Dilger, Ghali and Rao 1996).

## **CHAPTER III**

### **XFEM CRACK MODELING FOR FRACTURE OF CONCRETE**

Solid materials perform extensively varying load-displacement response when loaded until reaching to the failure point. In view of that, the appropriate category of material continuity must be considered for conducting a precise analysis of solid materials. The classical strength of materials theory and the plastic damage theory deal only with continuous fields or weak discontinuities. It became possible to model plasticity problems at large deformations by means of the Finite Element Method (FEM); however, with no strong discontinuities accounted for, FEM computations still lead to mesh dependent solutions.

The practice of plastic damage and fracture mechanics theories enable the achievement of more accurate solutions to engineering problems since they are capable of handling problems with strong discontinuities, where both displacement and strain fields are discontinuous through a crack surface (Figure 13). Therefore, combining classical fracture mechanics theories with FEM formulations by means of appropriate methods is essential for the correct solution of nonlinear problems. In this chapter, fundamentals of the linear elastic fracture mechanics and the nonlinear fracture mechanics theories will be reviewed, then the basic concepts of several modeling techniques including the Extended Finite Element Method (XFEM) will be introduced in order to explain the essentials of computational fracture modeling of concrete (Mohammadi 2008).

#### **3.1 Fracture Mechanics for Concrete**

Concrete is an inhomogeneous material with initial defects and imperfections such as entrapped air voids, defected aggregates, weak mortar-aggregate bonding and micro-cracks. These imperfections affect the structural response of concrete members significantly. The most important consequences of this heterogeneous and defective structure are the tension softening behavior of concrete and the lower tensile strength. The tension softening takes place in a region near the crack tip and is a relevant property, which controls the fracture characteristics of concrete. It is unlikely to obtain the true response of concrete structures by neglecting this behavior. Tensile strength of concrete is also an important parameter that

affects the structural response; however, it is usually neglected in calculations for the sake of simplicity (Shi 2009), (Asferg 2006).

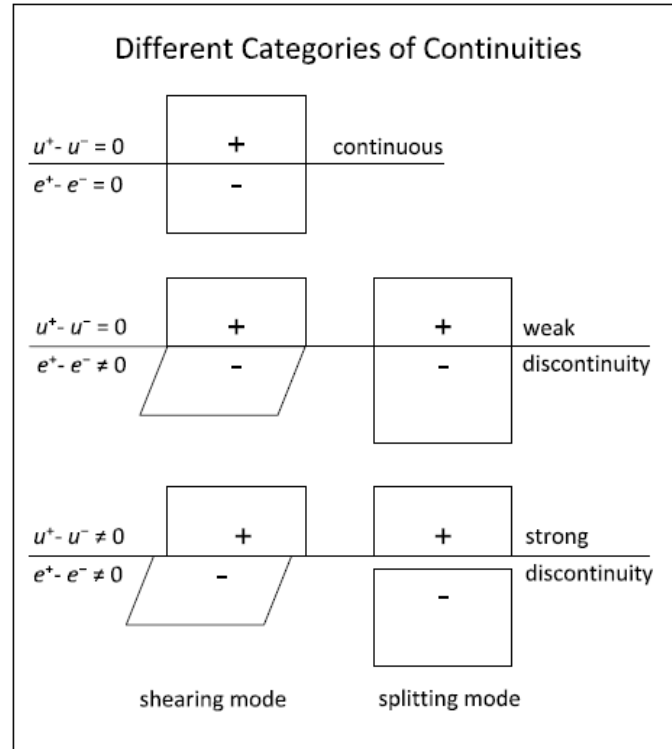


Figure 13: Different categories of continuities (Mohammadi 2008)

The abovementioned properties of concrete can be incorporated in analyses by use of fracture mechanics theories. Therefore, the practice of fracture mechanics is important for the structural analysis of concrete. A precise load-deformation response can be achieved by predicting the crack initiation and propagation in the calculations.

The report of ACI Committee 446 describes the fracture mechanics as a failure theory, which is based on energy and strength based criteria. It also explains that fracture mechanics considers the propagation of failure through the structure. The report emphasizes that, although the current building codes on concrete structures were prepared by ignoring fracture mechanics and has been used successfully until now, still there are reasons to incorporate failure theories into the structural codes. These reasons are listed in five topics by the Committee (ACI Committee 446 1991):

- The fracture initiation should be based on an energy based criterion instead of relying on a stress based one. Surface fracture energy of solid bodies can be used to derive an energy based measure of crack initiation.
- The calculations must give objective results regardless of the mesh sizes of finite element models or choice of coordinate systems, locations etc. (Figure 14). When the amount of energy dissipated per unit crack length is specified, it is possible to avoid such mesh dependent results.

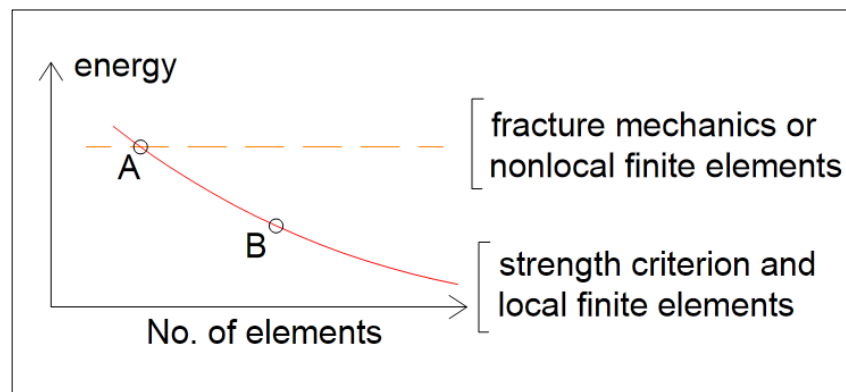


Figure 14: Spurious mesh sensitivity (ACI Committee 446 1991)

- The lack of a yield plateau in the load-deflection curve suggests that the subject material exhibits brittle softening behavior. That implies the propagation of the failure zone through the structure; hence the spread of failure should be tracked by use of fracture mechanics (Figure 15).
- The ductility and capability of absorbing energy for a material can be determined from the area under the load-deflection curve. For a material which exhibits softening behavior, the only way to calculate true ductility is to consider the post-peak response, in other words the nonlinearity in analyses.
- Calculations according to the classical theories may lead to different load-deflection responses in structures with different sizes. This phenomenon is called the size effect, and it has been overcome by using empirical formulas in the present structural codes. However, by means of the fracture mechanics theories, the size effect can be explained physically and the correct ductility level of concrete structures can be achieved.

These reasons, listed by ACI Committee 446, indicate the significance of fracture mechanics theories for concrete structures in predicting the true post peak load-deflection response, having mesh-independent results and eliminating the size effect (ACI Committee 446 1991).

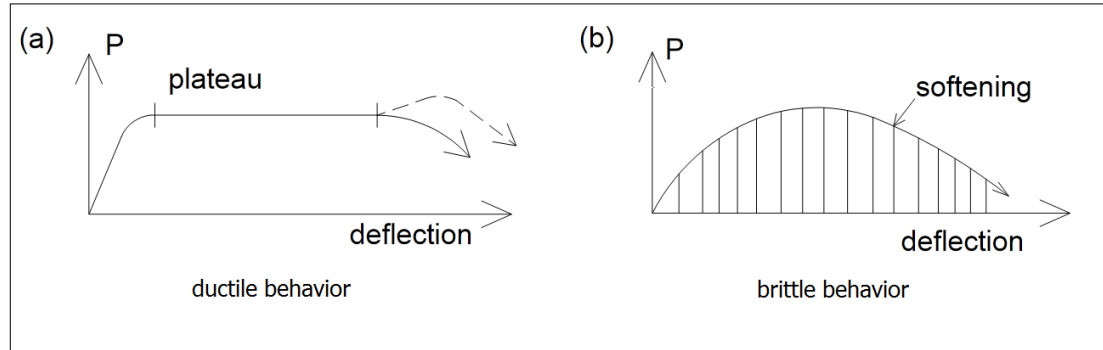


Figure 15: Load-deflection diagram of ductile and brittle structures (ACI Committee 446 1991)

### 3.1.1 Characteristic Fracture Properties of Concrete

Solid materials can be classified into three groups according to their fracture characteristics. These are brittle (glass-like materials), quasi-brittle (concrete and ceramics), and ductile materials (metals). Fracture characteristics are based on the type of material behavior in the boundary of fracture process zone (FPZ). FPZ, by definition, is the zone where the stresses normal to the crack surface decrease gradually by the increase of strains (Figure 16). In brittle materials, such as glass, fracture process takes place in a very small FPZ and the remaining parts possess linear-elastic behavior. Unlike brittle materials, plastic zone of quasi-brittle and ductile materials is larger thus has a nonlinear fracture response. FPZ of quasi-brittle materials is spread through the whole nonlinear zone, while ductile materials have a relatively small FPZ inside their perfectly plastic nonlinear zone (Figure 17). It is the main difference between quasi-brittle and ductile materials (ACI Committee 446 1991). Fracture characteristics of materials can be further classified in terms of the structure size,  $D$ , and the length of FPZ,  $l_p$ , as shown in Table 2.

Table 2: Appropriate Theories for Analyzing Failure (Bazant 2002)

For $D/l_p \geq 100$ :	Linear elastic fracture mechanics
For $5 \leq D/l_p < 100$ :	Nonlinear quasi-brittle fracture mechanics
For $D/l_p < 5$ :	Non-local damage, discrete element models, plasticity



In the course of fracture process of a concrete structure, aggregates together with hardened cement paste perform bridging function until they separate completely from each other. This is mainly because of the weak bonding between constituents of concrete leading to a separation mechanism rather than the failure of individual components. Micro-cracking due to the heterogeneous composition of concrete and the effect of bridging between paste and aggregates, together, induce a tension softening effect through the cracked surfaces. In Figure 16, the load-deformation curve of concrete is presented to show the softening behavior with corresponding points in FPZ. After the peak point is reached, crack surface proceed to have a descending stress transfer capacity up to a point where the crack is fully opened (Asferg 2006).

Starting with a crack bridging region and followed by a micro-cracking part, FPZ of concrete spread through a noticeably large area. With the inelastic fracture behavior inside this extended FPZ, concrete belongs to the quasi-brittle materials whose fracture must be investigated by nonlinear fracture mechanics.

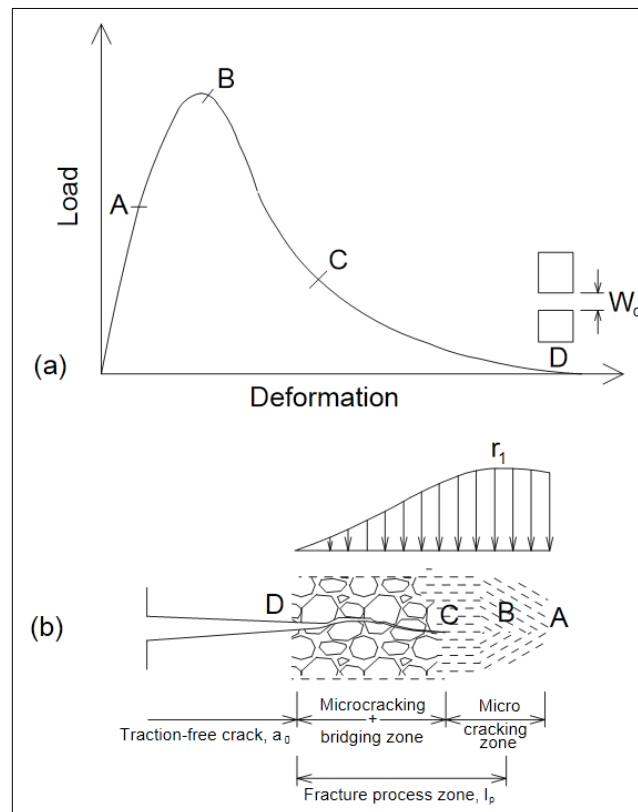


Figure 16: (a) Typical tensile load-deformation response and (b) illustration of the fracture process zone of concrete (Asferg 2006)

The approximate length of fracture process zone,  $l_p$ , for solid materials has been introduced by Irwin as depicted in Equation (1); where  $E$  is the modulus of elasticity,  $G_f$  is the fracture energy, and  $f_t$  is the tensile strength. There are some other formulations which have been derived specifically for predicting the FPZ length of concrete. One of them was proposed by Bazant and Oh, which suggests correlating the effective length and width of FPZ to the maximum aggregate size,  $d_a$ , of the subject concrete mixture. According to that assumption, fracture of three point bending specimens occurs in a zone with  $12d_a$  length and  $3d_a$  width (ACI Committee 446 1991).

$$l_p = \frac{E \times G_f}{f_t^2} \quad (1)$$

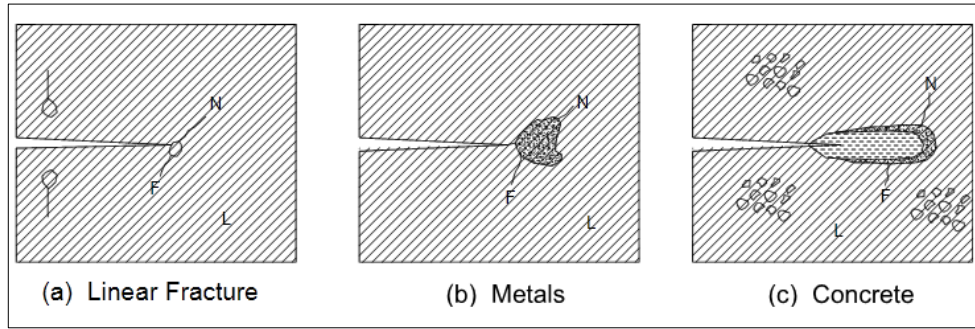


Figure 17: Linear zone (L), nonlinear zone (N) and fracture process zone (F) in fracture of different materials (ACI Committee 446 1991)

### 3.2 Introduction to Fracture Mechanics of Brittle Materials

The early theories of fracture mechanics were based on the linear elasticity with the assumption that while the failure process takes place at the crack tip, the other parts remain elastic. Reasonably, linear elastic theory could result in accurate solutions for brittle materials, since their fracture process occurs in an adequately small region. However, when the subject material of the fracture problem is not brittle, then the practice of the linear elastic fracture mechanics (LEFM) is not suitable because of the relatively larger FPZ of non-brittle materials. The investigated material in the scope of this thesis is concrete, and as mentioned before, concrete belongs to quasi-brittle type of materials thus is not compliant to linear elastic theory. However, the nonlinear fracture theories developed for concrete are also initiated from fundamentals of linear elastic fracture mechanics. So, basics of fracture mechanics will be introduced starting from the LEFM through the next topics.

### 3.2.1 Linear Elastic Fracture Mechanics (LEFM)

#### 3.2.1.1 Basic Elasticity Equations

In the Cartesian coordinate system, strain components can be defined in respect to the displacement components as follows:

$$\varepsilon_x = \frac{\partial u}{\partial x} ; \varepsilon_y = \frac{\partial v}{\partial y} ; \varepsilon_z = \frac{\partial \omega}{\partial z} ; \gamma_{xy} = \frac{\partial v}{\partial x} + \frac{\partial u}{\partial y} ; \gamma_{xz} = \frac{\partial \omega}{\partial x} + \frac{\partial u}{\partial z} ; \gamma_{yz} = \frac{\partial \omega}{\partial y} + \frac{\partial v}{\partial z} \quad (2)$$

In Eq. (2)  $u$ ,  $v$  and  $\omega$  stand for the displacement components in  $x$ ,  $y$  and  $z$  directions respectively; and  $\varepsilon_x, \varepsilon_y, \varepsilon_z, \gamma_{xy}, \gamma_{yz}, \gamma_{xz}$  are the strain components. In conjunction with strains, the stress components for isotropic materials are as follows according to the Hooke's Law:

$$\begin{aligned} \sigma_x &= \lambda(\varepsilon_x + \varepsilon_y + \varepsilon_z) + 2G\varepsilon_x \\ \sigma_y &= \lambda(\varepsilon_x + \varepsilon_y + \varepsilon_z) + 2G\varepsilon_y \\ \sigma_z &= \lambda(\varepsilon_x + \varepsilon_y + \varepsilon_z) + 2G\varepsilon_z \\ \tau_{xy} &= G\gamma_{xy} \\ \tau_{xz} &= G\gamma_{xz} \\ \tau_{yz} &= G\gamma_{yz} \end{aligned} \quad (3)$$

$\lambda$  and  $G$  are the Lamé constant and the shear modulus respectively and are defined as:

$$G = \frac{E}{2(1+\nu)} ; \lambda = \frac{\nu E}{(1+\nu)(1-2\nu)} \quad (4)$$

where  $E$  is the modulus of elasticity and  $\nu$  is the Poisson's ratio.

Three-dimensional elasticity problems can be simplified under certain assumptions regarding the loading conditions and geometry. The plane-stress assumption is used when thickness is very small compared to the other two dimensions; hence the displacement components do not vary and the stress component becomes zero in that dimension. The following simplified stress-strain relations are valid in case of plane-stress:

$$\begin{aligned} \sigma_x &= \lambda(\varepsilon_x + \varepsilon_y + \varepsilon_z) + 2G\varepsilon_x \\ \sigma_y &= \lambda(\varepsilon_x + \varepsilon_y + \varepsilon_z) + 2G\varepsilon_y \\ \sigma_z &= 0 \\ \tau_{xy} &= G\gamma_{xy} \\ \tau_{xz} &= \tau_{yz} = 0 ; \gamma_{xz} = \gamma_{yz} = 0 \\ \varepsilon_z &= -\frac{\lambda}{\lambda + 2G}(\varepsilon_x + \varepsilon_y) \end{aligned} \quad (5)$$

The plane-strain assumption is used to simplify problems when the thickness is significantly large as is the case with tunnel or dam cross-sections. The body forces or applied loads

cannot change nor have components along the third direction. Simplified stress-strain relations for the plane-strain case are given below:

$$\begin{aligned}
\sigma_x &= \lambda(\varepsilon_x + \varepsilon_y) + 2G\varepsilon_x \\
\sigma_y &= \lambda(\varepsilon_x + \varepsilon_y) + 2G\varepsilon_y \\
\sigma_z &= \lambda(\varepsilon_x + \varepsilon_y) \\
\tau_{xy} &= G\gamma_{xy} \\
\tau_{xz} = \tau_{yz} &= 0; \gamma_{xz} = \gamma_{yz} = 0 \\
\varepsilon_z &= 0
\end{aligned} \tag{6}$$

Most of the fundamental fracture mechanics laws were derived by using the given plane elasticity relations. Edge crack and central crack solutions on infinite plates are two popular examples to the plane elasticity solutions of fracture mechanics. The central crack problem, shown in the Figure 18, explores the formation of a central crack on an infinite plate. Solution to this problem by use of complex stress functions provides the elastic crack-tip stress field equations. Derivation of the crack-tip stress equations and the related complex stress functions will not be explained in this thesis; further information can be found in the referenced textbook by Zihai Shi (Shi 2009). The elastic crack-tip stress relations are presented in Equation (7) in case of the plate subjected to tension, and presented in Equation (8) for plate subjected to shear (Shi 2009). In these equations  $r$  is the crack-tip radius and,  $\theta$  is the angle between the crack-tip direction and the horizontal axis.

$$\begin{aligned}
\sigma_x &= \sigma \frac{\sqrt{a}}{\sqrt{2r}} \cos \frac{\theta}{2} \left( 1 - \sin \frac{\theta}{2} \sin \frac{3\theta}{2} \right) \\
\sigma_y &= \sigma \frac{\sqrt{a}}{\sqrt{2r}} \cos \frac{\theta}{2} \left( 1 + \sin \frac{\theta}{2} \sin \frac{3\theta}{2} \right) \\
\tau_{xy} &= \sigma \frac{\sqrt{a}}{\sqrt{2r}} \sin \frac{\theta}{2} \cos \frac{\theta}{2} \cos \frac{3\theta}{2}
\end{aligned} \tag{7}$$

$$\begin{aligned}
\sigma_x &= -\tau \frac{\sqrt{a}}{\sqrt{2r}} \sin \frac{\theta}{2} \left( 2 + \cos \frac{\theta}{2} \cos \frac{3\theta}{2} \right) \\
\sigma_y &= \tau \frac{\sqrt{a}}{\sqrt{2r}} \sin \frac{\theta}{2} \cos \frac{\theta}{2} \cos \frac{3\theta}{2} \\
\tau_{xy} &= \tau \frac{\sqrt{a}}{\sqrt{2r}} \cos \frac{\theta}{2} \left( 1 - \sin \frac{\theta}{2} \sin \frac{3\theta}{2} \right)
\end{aligned} \tag{8}$$

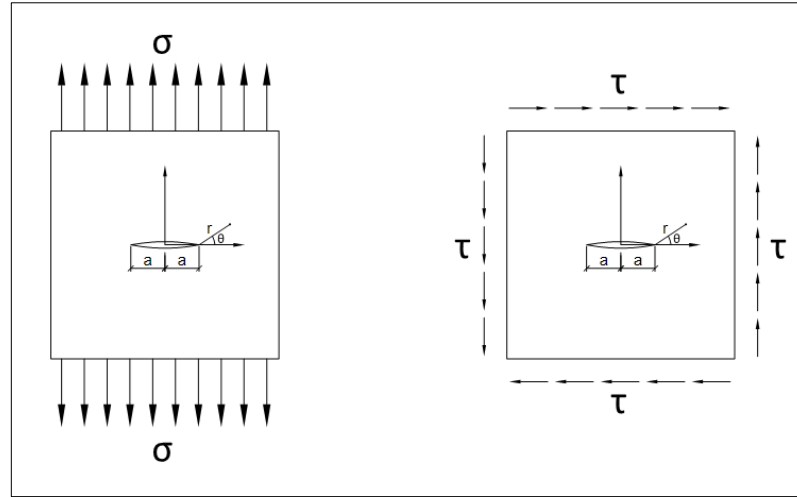


Figure 18: An infinite plate with a central crack subjected to tension (left), and subjected to shear (right) (Shi 2009)

### 3.2.1.2 Griffith Fracture Theory

Fracture mechanism of brittle materials has been studied since the early years of 19<sup>th</sup> century. Research on the LEFM initiated from the fact that fracture of brittle materials occurred at significantly lower stresses compared to the theoretical estimations of the fracture strength. After it was understood that the reason of lower actual fracture strength is due to the presence of flaws inside a solid body, Griffith clarified this case by suggesting an energy-based fracture principle for brittle materials (Mohammadi 2008).

The early theories of fracture mechanics was depended on the assumption that failure takes place at a single point near the crack tip. At that point the stress components approach to infinity as the crack tip radius decreases. This is called the stress singularity, and is the reason of computing infinitely large stress concentrations near crack tip, regardless of the scale of external loading. It was not possible to introduce a strength based failure criterion due to the stress singularity. The energy based fracture theory of Griffith enabled the derivation of crack initiation and propagation criteria for brittle materials. These criteria will be explained comprehensively in the upcoming parts (ACI Committee 446 1991).

Through a balance equation similar to the first law of thermodynamics, Griffith derived a fracture criterion by correlating the increase of crack length with the total change of energy inside the body. The first law of thermodynamics states that the rate of change of internal energy in a body is equal to the summation of supplied heat and the rate of work done by the system (Eq. (9)). Since fracture mechanics problems belong to quasi-static systems, the internal kinetic energy  $U_k$  and the heat flux  $Q$  become zero so they are vanished from the

equation (Eq. (10)). For a brittle fracture process, the conservation of energy required to develop a half-length crack ( $a$ ) can be derived as shown in Equation(11).The terms  $U_s$  and  $U_r$  in the Equation (11)represent internal strain energy and surface energy respectively, and  $W$  represents the work done by the loading(Mohammadi 2008).

$$\frac{d}{dt}(U_k + U_s + U_r) = \frac{d}{dt}(-W + Q) \quad (9)$$

$$U_k = Q = 0 \quad (10)$$

$$\frac{d}{da}(U_s + W + U_r) = 0 \quad (11)$$

The total potential energy,  $\Pi$ , of the system can be formulated as the sum of internal elastic strain energy and the work done by the outer loading (Eq. (13)).

$$\Pi = U_s + W \quad (12)$$

$$\frac{d}{da}W = -\frac{d}{da}(U_s + U_r) \quad (13)$$

If the  $W$  term from Equation (11) (the rearranged form is shown in Equation (13)) is substituted into the total potential energy equation (Eq.(12)) and differentiated with respect to the half crack length, then the amount of required energy dissipation for crack growth can be determined as shown in Equation (14).

$$\frac{\partial \Pi}{\partial a} = \frac{\partial U_s}{\partial a} - \frac{\partial U_s}{\partial a} - \frac{\partial U_r}{\partial a} = -\frac{\partial U_r}{\partial a} \quad (14)$$

Therefore, in case of an ideally brittle material, the total energy during fracture process becomes equal to only the surface energy of the system. Griffith has symbolized the surface energy by  $\gamma_s$ . Accordingly, the total energy becomes  $2\gamma_s$  since there are two surfaces involved during fracture of solid bodies (Eq. (15)) (Mohammadi 2008).

$$-\frac{\partial \Pi}{\partial a} = \frac{\partial U_r}{\partial a} = 2\gamma_s \quad (15)$$

### 3.2.1.3 Fracture Modes And Stress Intensity Factor

The idea behind solving a fracture problem is to determine the amplitude of the stresses near the crack tip, while being in line with the corresponding load and boundary conditions. Since the stress field is distributed similarly for all problems, the unique fracture characteristics are identified by means of the amplitude of stress fields specifies. Irwin has introduced the stress intensity factor (SIF) concept in order to represent this unique quantity.

Type of loading is an important factor that changes the displacement pattern of cracking and characteristics of the fracture process. There are three possible fracture modes in terms of the loading conditions (Figure 19). Mode I is the opening mode where the cracking is governed by loads which are normal to the crack surface. In Mode II, loading makes the crack surfaces slide through each other. That type of loading forms in-plane shear throughout the plane. The last mode is Mode III, tearing or out-of-plane shear loading; and is not valid for the plane elasticity.

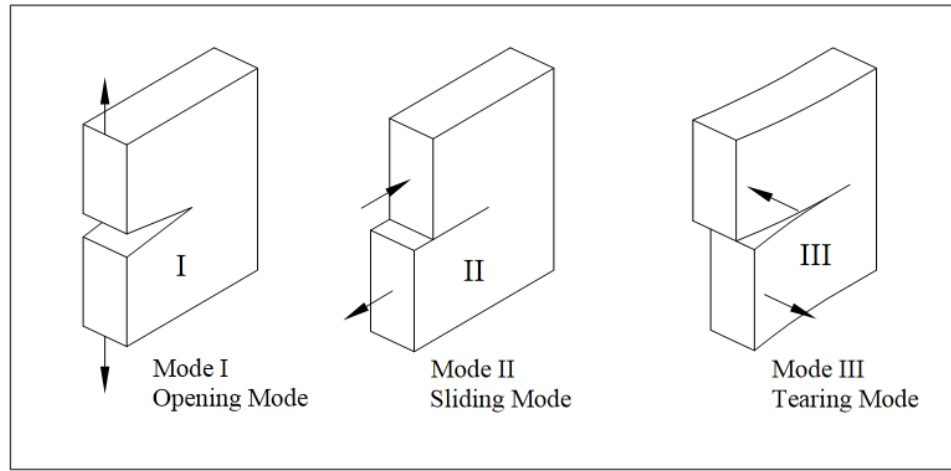


Figure 19: Modes of deformation at the crack-tip

In order to obtain accurate solutions to linear elastic fracture problems, the SIF has been defined separately for three modes of crack displacement. The notations for SIFs are  $K_I$ ,  $K_{II}$  and  $K_{III}$  for Mode I, Mode II and Mode III respectively. Assuming that the crack-tip radius tends to zero; crack-tip stress field equations, presented in equations (7) and (8), could be rearranged by using the following equalities:

$$K_I = \sigma\sqrt{\pi a}; K_{II} = \tau\sqrt{\pi a}$$

$a$ : half of crack length

(16)

Accordingly, the crack-tip stress field equations turn into:

Mode I:

$$\begin{aligned}\sigma_x &= \frac{K_I}{\sqrt{2\pi r}} \cos \frac{\theta}{2} \left( 1 - \sin \frac{\theta}{2} \sin \frac{3\theta}{2} \right) \\ \sigma_y &= \frac{K_I}{\sqrt{2\pi r}} \cos \frac{\theta}{2} \left( 1 + \sin \frac{\theta}{2} \sin \frac{3\theta}{2} \right) \\ \tau_{xy} &= \frac{K_I}{\sqrt{2\pi r}} \sin \frac{\theta}{2} \cos \frac{\theta}{2} \cos \frac{3\theta}{2}\end{aligned}\quad (17)$$

Mode II:

$$\begin{aligned}\sigma_x &= -\frac{K_{II}}{\sqrt{2\pi r}} \sin \frac{\theta}{2} \left( 2 + \cos \frac{\theta}{2} \cos \frac{3\theta}{2} \right) \\ \sigma_y &= \frac{K_{II}}{\sqrt{2\pi r}} \sin \frac{\theta}{2} \cos \frac{\theta}{2} \cos \frac{3\theta}{2} \\ \tau_{xy} &= \frac{K_{II}}{\sqrt{2\pi r}} \cos \frac{\theta}{2} \left( 1 - \sin \frac{\theta}{2} \sin \frac{3\theta}{2} \right)\end{aligned}\quad (18)$$

Mode III:

$$\begin{aligned}\sigma_x &= \sigma_y = \sigma_z = \tau_{xy} = 0 \\ \tau_{xz} &= -\frac{K_{III}}{\sqrt{2\pi r}} \sin \frac{\theta}{2} \\ \tau_{yz} &= \frac{K_{III}}{\sqrt{2\pi r}} \sin \frac{\theta}{2}\end{aligned}\quad (19)$$

Equation (16) indicates that the stress intensity factor is related to the applied load and the crack length. As those parameters increase, both the value of stress intensity factor and the rate of stress development at the crack-tip become larger. Taking account of these relations, the stress intensity factors for three modes of fracture could be summarized as depicted in equation (20).

$$\begin{aligned}K_I &= \lim_{r \rightarrow 0} \sqrt{2\pi r \sigma_y(r, \theta = 0)} \\ K_{II} &= \lim_{r \rightarrow 0} \sqrt{2\pi r \tau_{xy}(r, \theta = 0)} \\ K_{III} &= \lim_{r \rightarrow 0} \sqrt{2\pi r \tau_{yz}(r, \theta = 0)}\end{aligned}\quad (20)$$

Using the concept of stress intensity factor, the deformation mode of cracking and the strength of stress singularity in the vicinity of crack-tip can be calculated. Having the K value obtained, the stress, strain and displacement components could be acquired by the simplified equations. Also, if the subject material is loaded by more than one configuration, then the introduced modes could be linearly superposed so as to achieve the crack-tip stress fields. That kind of fracture is called the mixed-mode cracking.

#### 3.2.1.4 Crack Propagation Criteria

As per the energy based theories of fracture, the formation of a crack is dependent on the amount of provided elastic energy by the applied external loads. Fracture happens when the



internal energy exceeds the critical fracture energy of the material. Accordingly, the Griffith Fracture Criterion for the growth of a sharp crack with a length of  $2a$  is defined as depicted below in Equation (21).

As it is mentioned before, the LEFM theories are only valid for perfectly brittle materials. Therefore the fracture criterion in Equation (21) does not fit to the real problems. Regarding the contribution of friction induced energy dissipation during fracture, Irwin has replaced the  $\gamma_s$  term by the energy release rate. Energy release rate is symbolized by the letter  $G$ , and is a measure for the quantity of energy dissipation required for unit length of crack propagation (Shi 2009). Fracture begins when  $G$  reaches its critical value which is denoted by  $G_c$ . This critical value is also known as the material toughness, and another fracture criterion can be written by substituting  $G_c$  into Equation (21) (Eq. (22)) (Asferg 2006).

$$\begin{aligned} \frac{\pi a \sigma_c^2}{E} &= 2\gamma_s; \sigma_c = \sqrt{\frac{2\gamma_s E}{\pi a}} \text{ (for plane stress)} \\ \sigma_c &= \sqrt{\frac{2\gamma_s E}{(1-\nu^2)\pi a}} \text{ (for plane strain)} \end{aligned} \quad (21)$$

One more fracture criterion within the context of LEFM can be derived with respect to the concept of stress intensity factors, which is mentioned before. The critical intensity factors are defined distinctly for three fracture modes, and denoted as  $K_{Ic}$ ,  $K_{IIc}$  and  $K_{IIIc}$ . In that case, the condition for initiation and propagation of a Mode I type crack is  $K_I > K_{Ic}$ . Furthermore, the critical energy release rate,  $G_c$ , and the critical SIF can be associated by substituting Equation (16) into Equation (22). By this way the equality in Equation (23) could be obtained.

$$\begin{aligned} \frac{\pi a \sigma_c^2}{E} &= 2\gamma_s = G_c, \sigma_c = \sqrt{\frac{G_c E}{\pi a}} \text{ (for plane stress)} \\ \sigma_c &= \sqrt{\frac{G_c E}{(1-\nu^2)\pi a}} \text{ (for plane strain)} \end{aligned} \quad (22)$$

$$K_{Ic}^2 = E G_c \quad (23)$$

### 3.2.2 Nonlinear Fracture Mechanics (NLFM)

According to LEFM theories, energy dissipation takes place at one point during fracture. With this assumption, infinite stresses are calculated at crack tip which is not possible in reality. Therefore, LEFM solutions lead to inaccurate results as the investigated type of material diverges from ideal brittleness. As mentioned before, concrete belongs to quasi-brittle

materials with its tension softening behavior and an extended FPZ, thus fracture of which should not be examined by LEFM. Researchers have introduced several models in order to obtain more realistic results for nonlinear fracture problems. The first models which suited for the concrete fracture were cohesive zone models proposed by Dugdale and Barenblatt.

### 3.2.2.1 Cohesive Zone Models

Cohesive crack models are developed by incorporating plastic zones nearby the crack tips. It is assumed that there are closing forces acting against crack opening along these plastic zones. They form a traction-separation behavior in the crack tip. By this means, smooth crack closure is obtained, rather than the formation of sharp crack edges where stress singularity occurs. The closure stresses are assumed to be equal to material's yielding stress,  $\sigma_{yld}$ , in Dugdale's cohesive model. Alternatively, Barenblatt proposed a varying stress distribution along the plastic length of crack (Shi 2009) (Figure 20).

These pioneering models for nonlinear fracture mechanics have introduced approximations to determine the extent of the plastic zone. To explain the approximations, the half-length of crack is denoted as  $c$ , then  $c$  is equal to the sum of plastic zone length ( $\rho$ ) and the traction-free crack length ( $a$ ) (Eq. (24)).

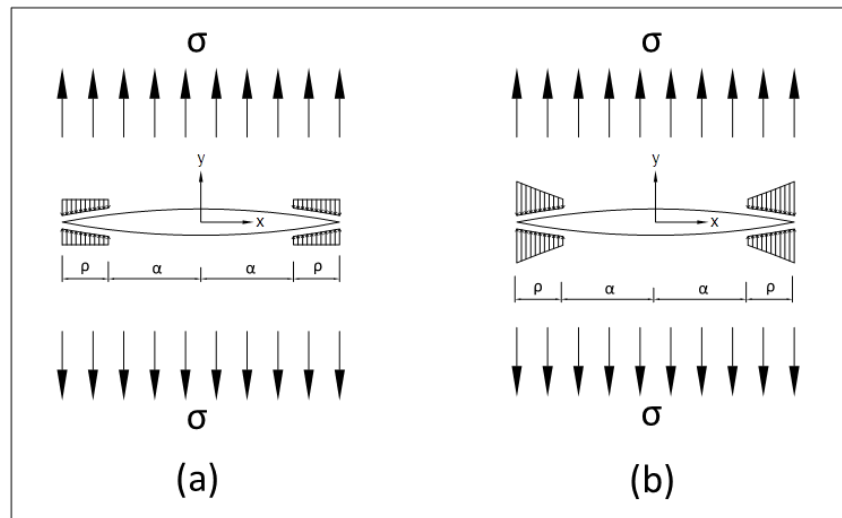
$$c = a + \rho \quad (24)$$

Afterwards, the length of the plastic zone can be determined based on the assumption that negative cohesive closure stresses (equal to yield stress of material) would cancel the stress intensity factor in the crack tip (Eq. (25)) (Asferg 2006).

$$K + K_{yld} = 0 ; \frac{c}{a} = 1 - \left( \cos \frac{\pi \sigma}{2 \sigma_{yld}} \right) \quad (25)$$

The concept of cohesive crack modeling was successfully used for concrete fracture in fictitious crack model (FCM) by Hillerborg. The development of cohesive stresses in FPZ was explained thoroughly in this model. Hillerborg has correlated the cohesive traction stresses with the crack opening displacement (COD). As seen in Figure 21, stresses are defined as a function of COD (Eq. (26)); where  $\omega$  is used to symbolize COD and  $\sigma$  for traction stresses. The fictitious part of crack terminates where COD reaches a critical value ( $\omega_c$ ); the crack surface becomes traction-free and linear elastic beyond this critical point. The critical crack opening displacement,  $\omega_c$ , has been obtained as approximately 160  $\mu\text{m}$  after numerous experimental studies had performed in order to explore concrete fracture parameters (Shi 2009).

$$\sigma = f(\omega) \quad (26)$$



There are several assumptions for calculating the concrete fracture energy based on experimental studies in the literature. However, the most direct approach is to equalize the area under the softening curve to the fracture energy (Eq. (27)) (Bazant 2002).

$$G_f = \int_0^{w_c} \sigma(w) dw \quad (27)$$

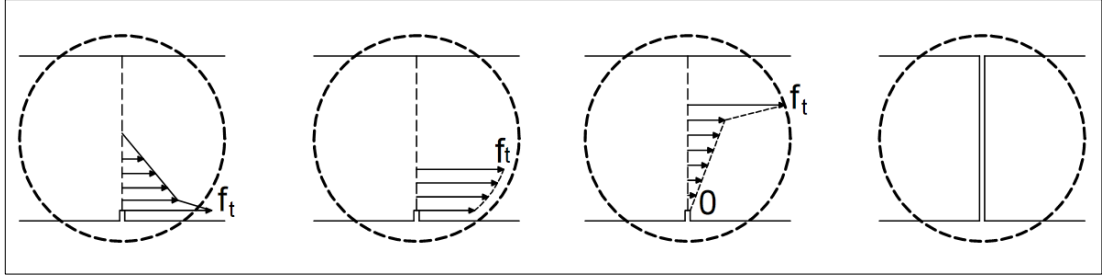


Figure 22: Development phases of FPZ (Shi 2009)

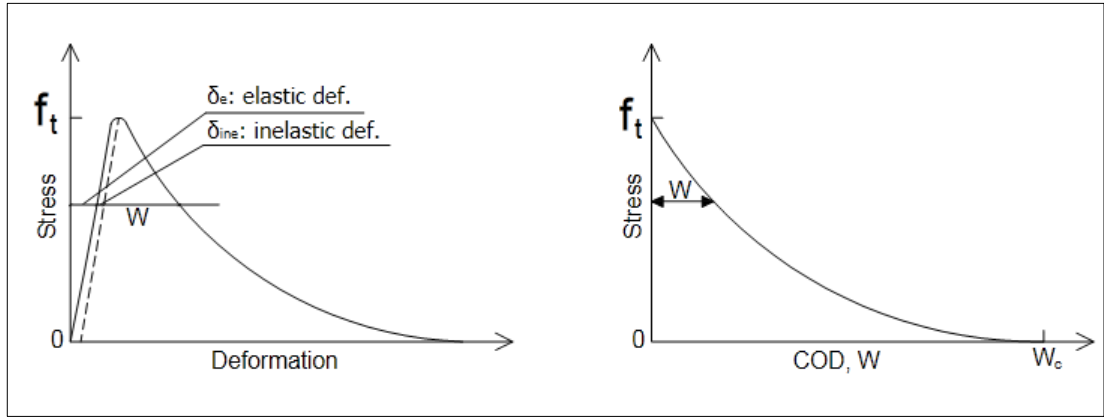


Figure 23: Load-deformation curve and tension softening curve (Shi 2009)

The crack band model (CBM) is an alternative model to FCM which takes the softening behavior into account in a different manner. CBM, introduced by Bazant and Cedolin, assumes a micro-cracking zone, which is spread in a band with certain thickness,  $h_c$ . The effect of cracking is modeled by a stress-strain curve (Figure 24) (Asferg 2006).

Therefore, COD is obtained as the product of fracture strain and crack band width. Similar to the FCM, fracture energy of concrete becomes equal to the area enclosed by this curve multiplied by  $h_c$  (Asferg 2006).

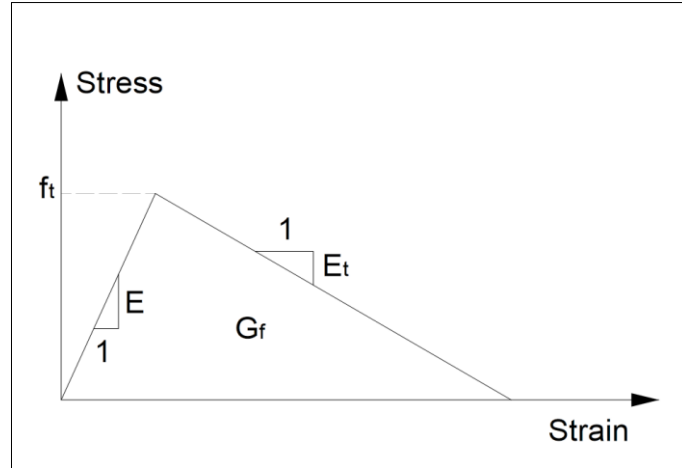


Figure 24: CBM stress-strain curve for crack propagation (Asferg 2006)

### 3.3 Crack Modeling Techniques for Concrete Fracture

Until this point, it is emphasized that cracking of concrete must be treated as a nonlinear fracture mechanics problem. Two basic modeling approaches are introduced for implementing nonlinear response of concrete; however, methods have not been mentioned yet. This part will provide fundamental information about some of the modeling techniques for fracture problems. In this manner, the progress of crack modeling beginning with simple but problematic models, continuing to development of superior techniques such as XFEM could be better understood.

#### 3.3.1 Local and Non-Local Models for Crack Propagation Analysis

The earliest attempts to solve a crack problem through the finite element method were based on assigning strength criteria to integration points of the elements. Cracks were formed when stresses calculated at an integration point exceed the corresponding strength of that point. However, it was revealed that local models have led to mesh dependent results. Researchers tried to overcome this problem by developing non-local models. Surrounding points were also involved in non-local models for determination of strength criteria rather than relying on a single point (Mohammadi 2008).

### 3.3.2 Smeared Crack Model

Smeared crack modeling is another approach for fracture mechanics problems. This approach is based on modeling the influence of cracking, rather than modeling cracks physically (Figure 25). In this case, smeared models are not capable of estimating crack geometry or crack width individually. The overall amount of strain which is induced by cracking,  $\varepsilon_{cr}$ , is added to the elastic strain,  $\varepsilon_e$ , to calculate the total strain. Then surface normal traction stresses are correlated to the cracking strains as depicted in Equation (28).

$$\varepsilon = \varepsilon_e + \varepsilon_{cr} ; \sigma = f(\varepsilon_{cr}) \quad (28)$$

In some crack modeling techniques, remeshing of the domain is required as the crack propagates. Since remeshing is a complicated and time consuming process, the smeared crack models are advantageous in terms of not needing remeshing. Although smeared models constitute a better alternative for crack modeling than local and non-local models, they have some difficulties as well. Besides the lack of crack geometry prediction, smeared models could lead to mesh dependent solutions due to the relation between the width of crack band and the chosen element size. One more serious problem is the possible false estimation of softening behavior (Asferg 2006).

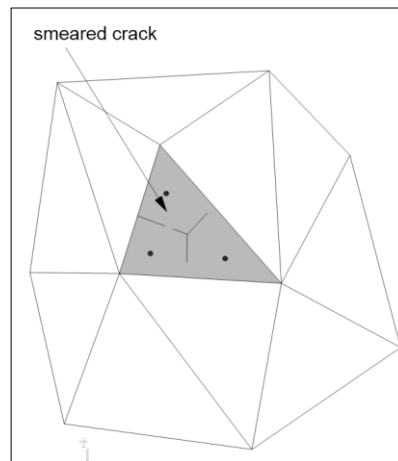


Figure 25: Illustration of a smeared crack (Mohammadi 2008)

### 3.3.3 Discrete Interface Crack Model

Unlike the smeared modeling approach, discrete crack models are able to physically simulate the crack geometry. In a discrete element model, cracks are located between elements, and cannot propagate through elements. Therefore, this kind of modeling is only useful with

predefined crack-paths. Modeling a crack-propagation problem with discrete interface crack model is not practical, since it requires changing the mesh geometry at every stage of the analysis. In addition, it is quite likely to have mesh-dependent results (Mohammadi 2008).

#### **3.3.4 Discrete Cracked-Element Model**

Discrete cracked-element models were developed by enabling the crack propagation through elements. To this end, remeshing procedures have been used to further discretize the cracked element ensuring the compatibility conditions. This technique provided a successful way to analyze crack propagation; however, again, it requires much effort and time for accomplishing the remeshing processes (Mohammadi 2008).

#### **3.3.5 Enriched Elements and Other Techniques**

As it is seen from the preceding parts, the most challenging problem in crack modeling is to avoid unreliable mesh-dependent solutions. Some of the abovementioned techniques give reasonable results, but they usually need remeshing process and demand a huge effort. There are also other methods for crack analyses such as the Element-Free Galerkin Method (EFGM) and the use of singular elements. Both methods have some disadvantages though. The formulation of EFGM does not need the discretization of the problem domain; hence, the mesh-related problems disappear. However, use of this method within the classical FEM formulation is not likely, therefore, computer based modeling is difficult to be used. On the other hand, the use of singular elements in FEM formulation is achievable and this method has enabled the crack modeling by only moving element nodes as to the crack formation. Singular elements removed the necessity of remeshing and resulted in objective results; nevertheless, it is not capable of modeling discontinuities. Therefore, to model the crack geometry, one should use the singular elements together with a discrete model formulation. In this case, the same problems, such as the impracticability of remeshing appear (Mohammadi 2008).

Embedded crack models have also been used in crack modeling analyses. Being a discrete approach, these models enable the crack propagation independently through an existing mesh. But, the obtained results are usually influenced by coupled strain fields through crack surface, which lead to a spurious estimation of softening response (Asferg 2006).

The aforementioned difficulties in modeling fracture mechanics problems created the need for a more convenient method that can be used to model crack propagation. In late 1990s modeling techniques based on enriched elements were introduced. These techniques have facilitated the solution to crack propagation analyses, especially for the nonlinear fracture mechanics problems.

The enriched elements are formed by using special shape functions within the classical finite element formulation. Discontinuities are modeled by means of these enriched shape functions; therefore, cracks are formed inside elements. So, the mesh geometry does not have to fit to the crack geometry. As a result, the same mesh geometry can be used for different set of problems, and no remeshing process is demanded (Mohammadi 2008). The most popular method with enriched elements is the Extended Finite Element Method (XFEM), which is the subject of the next part.

### 3.4 The Extended Finite Element Method (XFEM)

The Extended Finite Element Method (XFEM) was developed by incorporation of the enrichment functions into the classical FEM formulations. This was achieved by use of partition of unity property of finite elements. Discontinuous fields due to fracture can be modeled regardless of the mesh geometry, thus cracks can propagate independently without need of remeshing (Moës and Belytschko 2002).

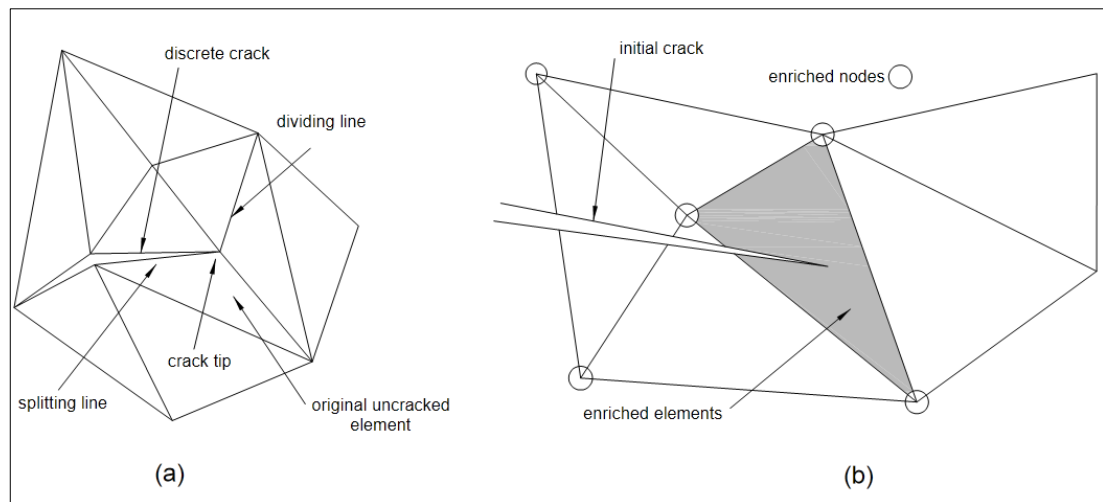


Figure 26: (a) Discrete cracked element (b) Enriched element: crack can propagate through the elements regardless of the mesh geometry (Mohammadi 2008)

Belytschko and Black are amongst the pioneering researchers in the development of XFEM, and they have listed three unique advantages of the method as follows:

- Since XFEM is a finite element method, technology and software that have been developed for finite element method can be used for XFEM analyses.
- XFEM is applicable to nonlinear problems.



- Need for remeshing is usually eliminated, also mesh does not have to match the geometry of discontinuity (Belytschko and Black 1999, Turkish Standards Institution 2000).

In XFEM formulation, discontinuities are defined inside the finite elements. This is realized by decomposing the displacement field into continuous and discontinuous parts. Consequently, crack propagation, independent of meshing, can be successfully modeled with fully uncoupled crack surfaces.

### 3.4.1 XFEM Formulation

The XFEM formulation consists of two enrichment parts added to the main shape functions to model the discontinuity; the first part is for the enrichment of nodes corresponding to the crack interior, and the second part is for the crack tip enrichment (Figure 27). The general XFEM formulation appears to be as depicted in Equation (29) (Dolbow , Moës and Belytschko 2000).

$$u^h(x) = \sum_I N_I u_I + \sum_J N_J H(x) b_J + \sum_{k \in K} N_k \left( \sum_{l=1}^4 c_k^l F_l(x) \right) \quad (29)$$

In Equation (29), "I" represents the set of nodes that belong to the continuous domain, where cracking does not occur. The second part, "J", is the set of nodes intersected by cracking, and finally "K" contains the nodes which surround the crack tips. The nodal degrees of freedom are included by the terms  $u_I$ ,  $b_J$  and  $c_k$  in terms of displacements.  $H(x)$  and  $F(x)$  are the enrichment functions for modeling the discontinuity. Definition of the jump function across the crack surface,  $H(x)$ , is as follows:

$$H(x) = \begin{cases} 1, & (x - x^*) \cdot n > 0 \\ -1, & \text{otherwise} \end{cases} \quad (30)$$

The closest point to  $x$  on crack is denoted as  $x^*$ , and the unit outward normal as  $n$ . This equation basically means that  $H(x)$  is equal to 1 above the crack; and -1 below the crack, implying the discontinuity (Figure 28). The function  $F(x)$  is for the enrichment of crack tip fields, and defined with respect to the local polar coordinates  $(r, \theta)$ .  $F(x)$  is as follows for a plane elasticity problem:

$$\{F_l(r, \theta)\}_{l=1}^4 = \left\{ \sqrt{r} \sin\left(\frac{\theta}{2}\right), \sqrt{r} \cos\left(\frac{\theta}{2}\right), \sqrt{r} \sin\left(\frac{\theta}{2}\right) \sin(\theta), \sqrt{r} \cos\left(\frac{\theta}{2}\right) \sin(\theta) \right\} \quad (31)$$

The first term of the crack tip function provides the discontinuous solution across the crack surface, while the remaining three terms provide the continuous asymptotic crack tip solution (Dolbow , Moës and Belytschko 2000), (Stolarska, et al. 2001), (ABAQUS 6.10 2010).

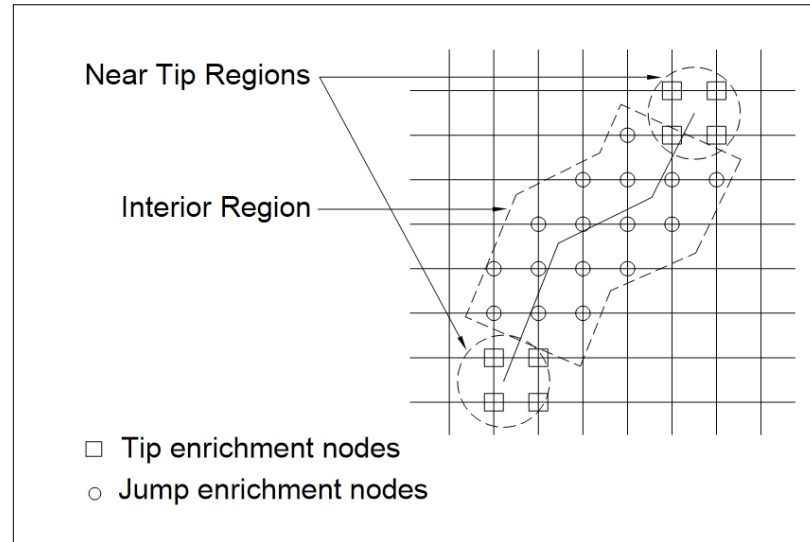


Figure 27: Regions of a crack for enrichment (Dolbow , Moës and Belytschko 2000)

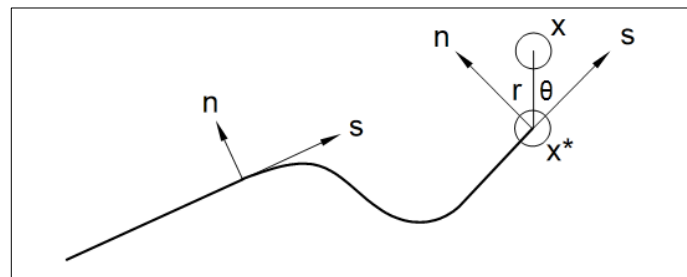


Figure 28: Illustration of normal and tangential coordinates for a smooth crack (ABAQUS 6.10 2010).

During crack propagation in an XFEM model, when the crack path passes through an edge, the nodes on the cut edge are enriched by two degrees of freedom in addition to the existing two classical degrees of freedom (Mohammadi 2008).

### 3.4.2 Cohesive Crack Growth with XFEM

As it was discussed before, the use of cohesive crack models is the most convenient method of modeling fracture problems of concrete and the other quasi-brittle materials. With the purpose of using XFEM for cohesive crack growth, the formulations, which are explained above, can be derived with regard to a modified domain (Figure 29) so as to include the cohesive traction stresses in the crack-tip zone.

For a cohesive crack growth, only displacement degrees of freedom are involved for accounting the smooth crack closure. Accordingly the jump functions, which define the deformation through the crack surface, are connected to the traction stresses of the fracture process zone in order to simulate the cohesive behavior. In the XFEM formulation, the effect of cohesive forces is accounted for together with the work done by external forces (Mohammadi 2008). A more detailed explanation of cohesive crack growth application can be found in referenced papers by Zi (Zi and Belytschko 2003) and Moës (Moës and Belytschko 2002).

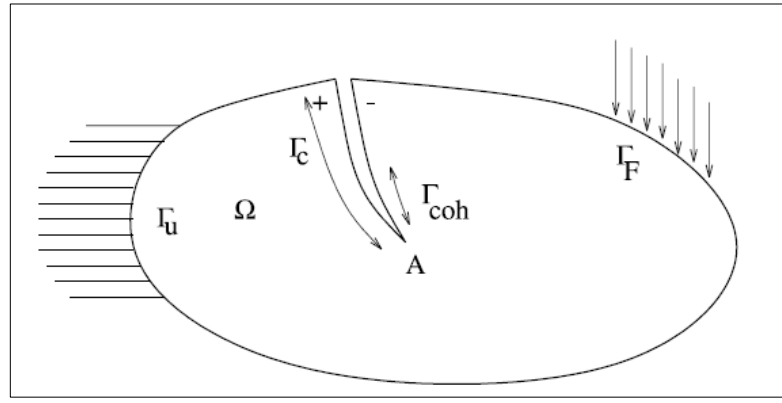


Figure 29: Domain with a crack involving cohesive zone (Moës and Belytschko 2002)

### 3.4.3 The Level Set Method

Since the crack propagation analyses are performed independently of the mesh geometry in XFEM, the formation of crack path and geometry is achieved by use of an additional numerical method which is called the level set method.

The level set function divides the domain into two non-overlapping subdomains whose interface represents the discontinuity (Figure 30). The interface is located at the zero level set of the function. Consequently, the level set function has opposite signed values at the two sides of this interface. The general definition of the level set function is as follows:

$$\phi(x) = \begin{cases} > 0, & x \in \Omega_1 \\ = 0, & x \in \Gamma \\ < 0, & x \in \Omega_2 \end{cases} \quad (32)$$

where  $\Omega_1$  and  $\Omega_2$  are the opposite signed subdomains, and  $\Gamma$  is the interface. The level set function,  $\phi(x)$ , can also be defined as a signed distance function as shown in Equation (33) where  $d$  stands for the normal distance of  $x$  to the interface (Mohammadi 2008).

$$\phi(x) = \begin{cases} d, & x \in \Omega_1 \\ -d, & x \in \Omega_2 \end{cases} \quad (33)$$

Beyond the two-dimensional domains, a single level set function is not sufficient to track discontinuities. For tracking the crack propagation, the crack surface is defined as the zero level set of a function  $\psi(x)$ . Next, an orthogonal function  $\phi(x)$  is defined and the intersection of level sets of these functions constitutes the crack geometry (Figure 31)(M. Stolarska, D. Chopp, et al. 2001)(ABAQUS 6.10 2010).

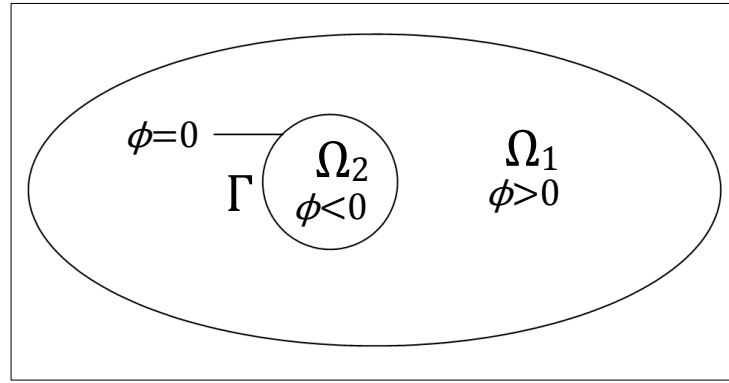


Figure 30: Definition of the level set function (Mohammadi 2008)

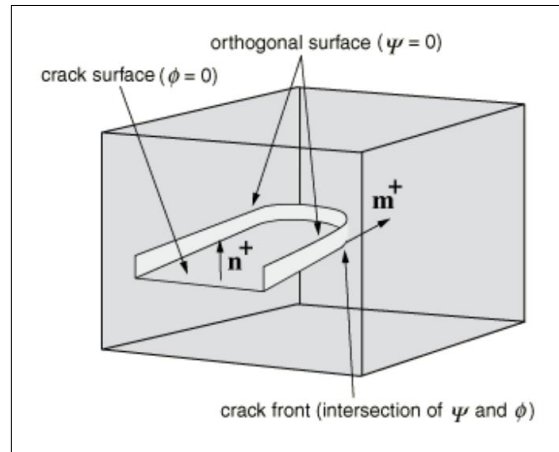


Figure 31: Representation of a non-planar crack in three-dimensions by two level set functions (ABAQUS 6.10 2010)

The calculated values of level set functions for representing the crack propagation is stored in the nodes of finite elements. Therefore, the level set algorithm can be easily used together with the finite element formulation. Furthermore, the level set algorithm does not cause a great computational effort since the functions are only required to be updated near the crack-tips. The remaining parts of the crack surface do not move or change as the crack propagation continues (M. Stolarska, D. Chopp, et al. 2001).

#### 3.4.4 Crack Propagation Analysis Example with XFEM in ABAQUS

In this part, results of two crack propagation analyses are presented. The purpose of these analyses is to show that the XFEM tool of ABAQUS can be successfully used to achieve acceptable cohesive crack propagation results. To this end, two-dimensional benchmark problems from the referenced textbook (Mohammadi 2008) is modeled via ABAQUS.

##### BEAM BENDING PROBLEM WITH ASYMMETRIC LOADING

The first XFEM model, which represents an asymmetric loading case of a beam, is constructed based on geometry, loading conditions and boundary conditions shown in Figure 32. The same material properties which defined in the textbook are used in the model. Assignment of the material properties and fracture mechanics parameters to prepare an XFEM model in ABAQUS will be explained comprehensively in the next chapter. The expected crack propagation pattern is shown in Figure 33.

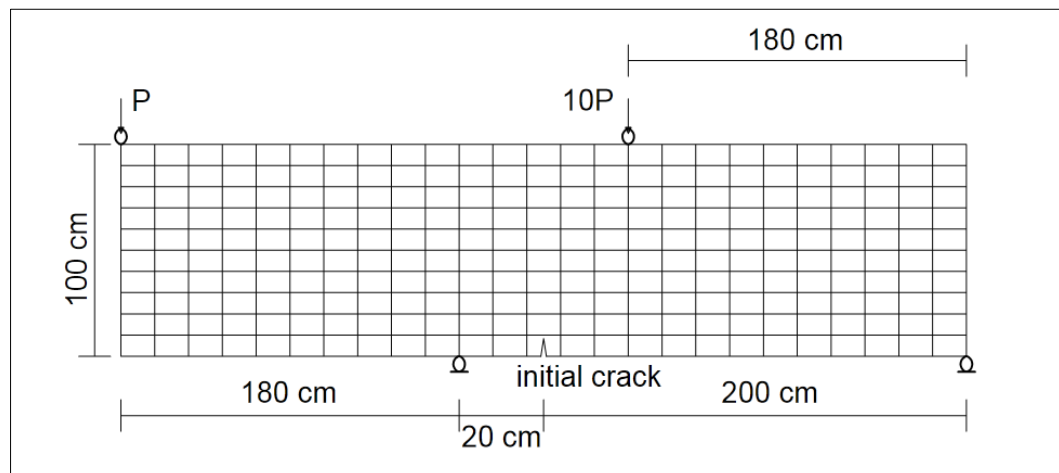


Figure 32: Geometry of the benchmark problem (Mohammadi 2008)

The mesh geometry and the boundary conditions of the XFEM model are shown in Figure 34. The XFEM analysis has been performed and the crack propagation pattern is depicted in Figure 35. When the results of the crack propagation analysis (Figure 35) and the expected crack propagation (Figure 33) are compared, it is seen that an accurate prediction of crack path has been achieved by the ABAQUS model.

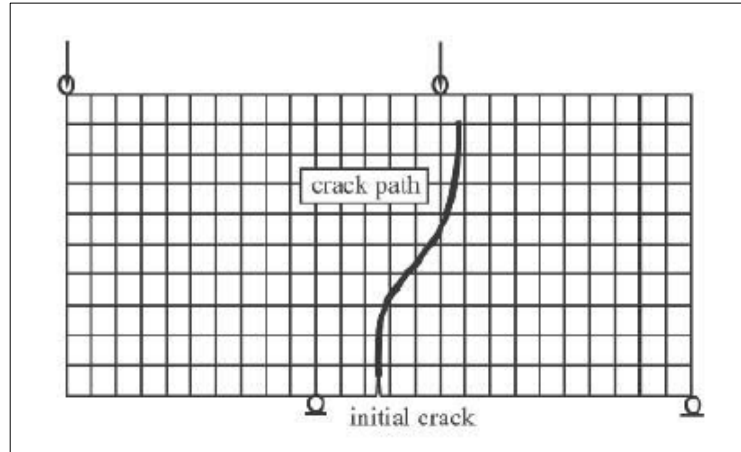


Figure 33: The expected crack propagation pattern (Mohammadi 2008)

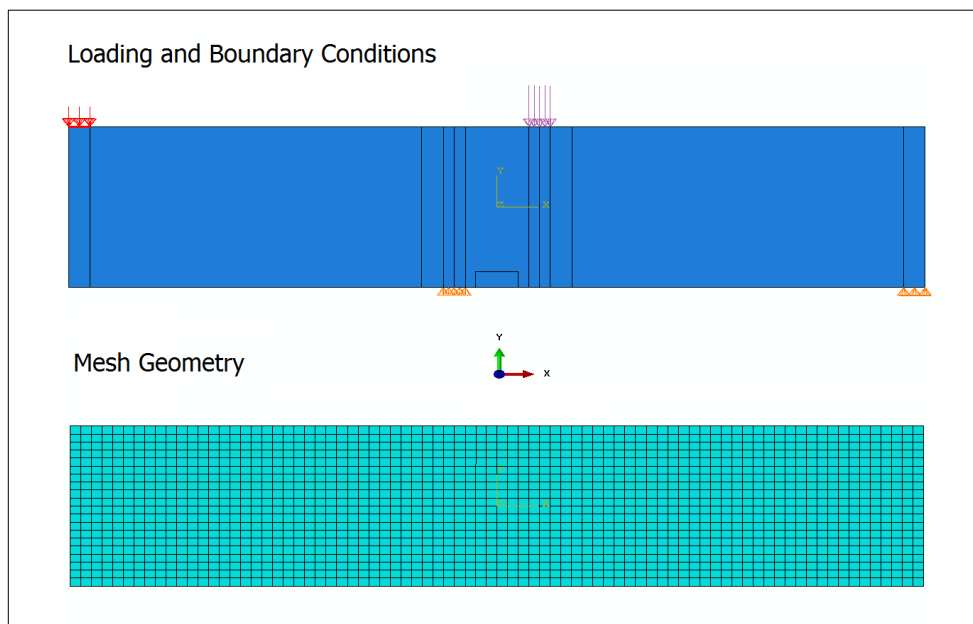


Figure 34: Loading / boundary conditions and mesh geometry of the XFEM model

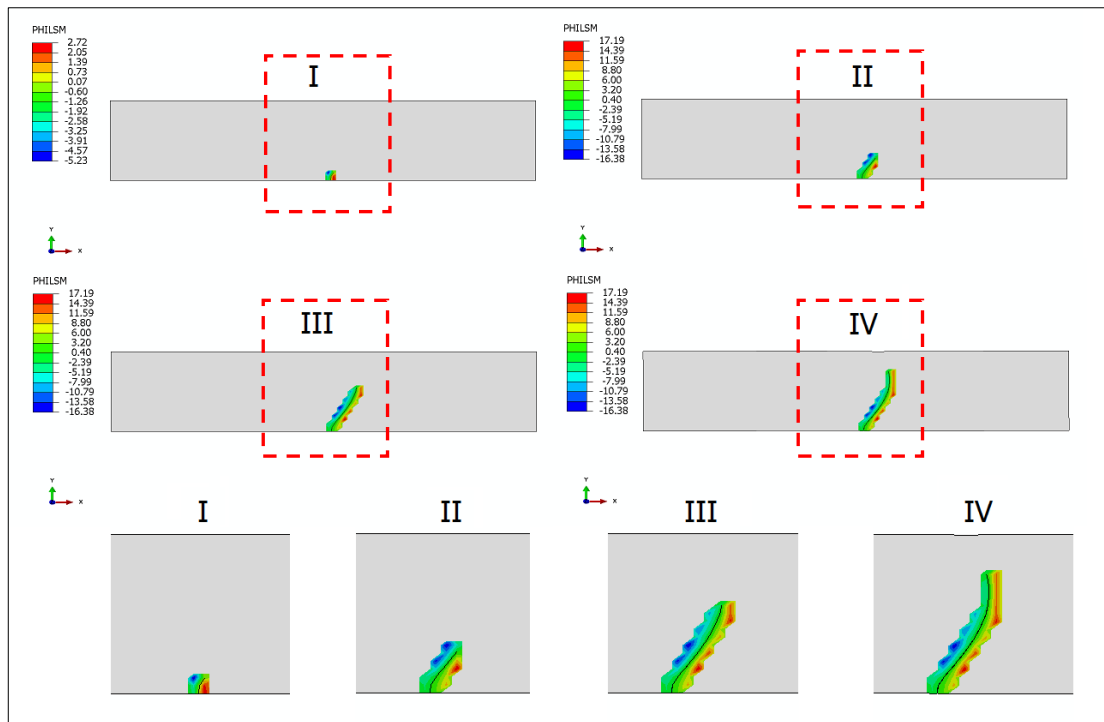


Figure 35: Crack propagation pattern of the XFEM analysis with level set contours

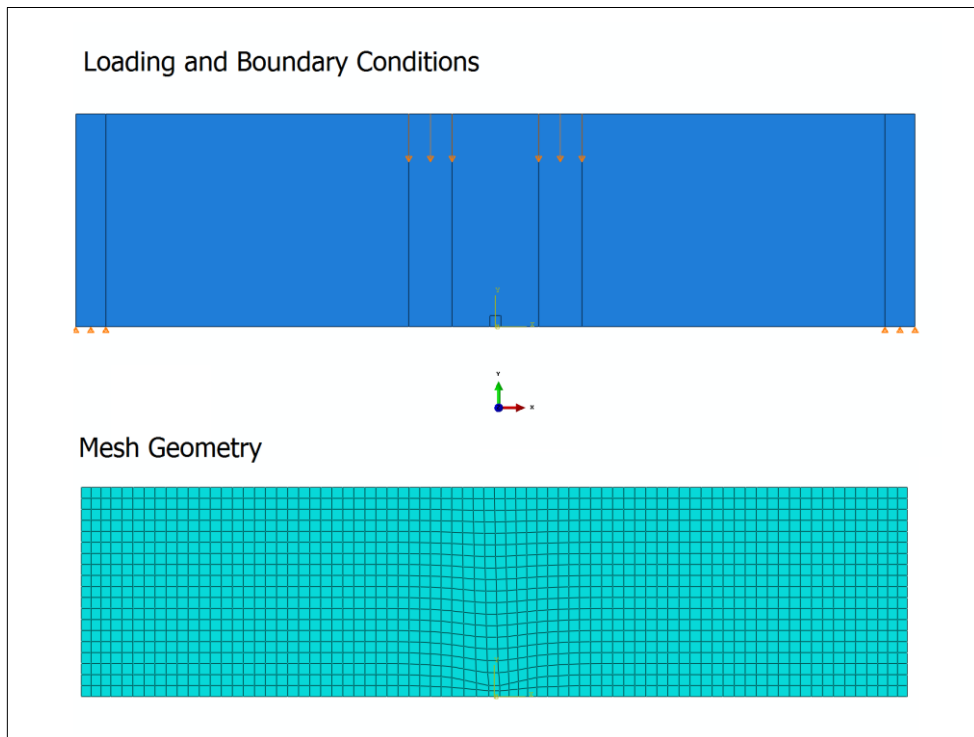


Figure 36: Loading / boundary conditions and mesh geometry of the XFEM model

## FOUR-POINT BEAM BENDING PROBLEM

The solution of another example problem from the same textbook (Mohammadi 2008) is presented in this part. ABAQUS analysis model of the problem is constructed by using the boundary and loading conditions which are shown in Figure 36. The acquired deformed and cracked shape of the beam is depicted in Figure 37.

In this example solution, it is aimed to provide not only the crack path, but also the load-displacement curve of the fracture process. In that way, the softening behavior of the material can be seen from the provided load-displacement curve (Figure 38). It is possible to compare the obtained curve with the load-displacement curve presented in the referenced textbook (Figure 39). The comparison of these two curves indicates that the cohesive crack model can be effectively applied by using XFEM within ABAQUS software.

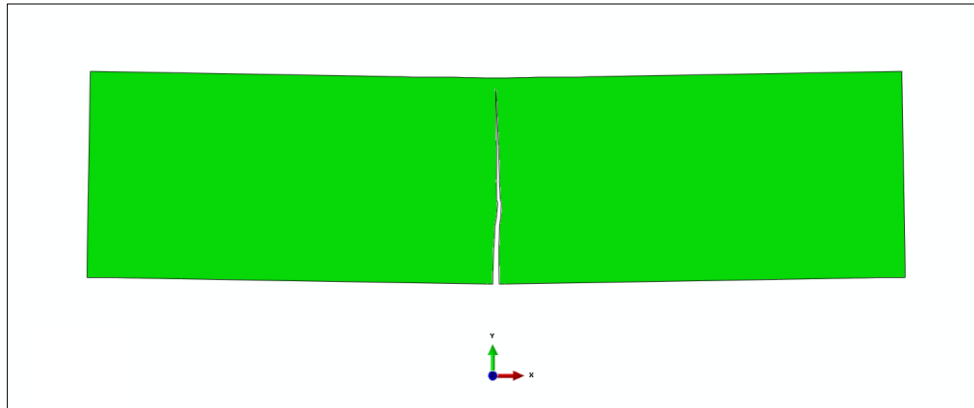


Figure 37: Crack propagation pattern of the four-point bending beam example

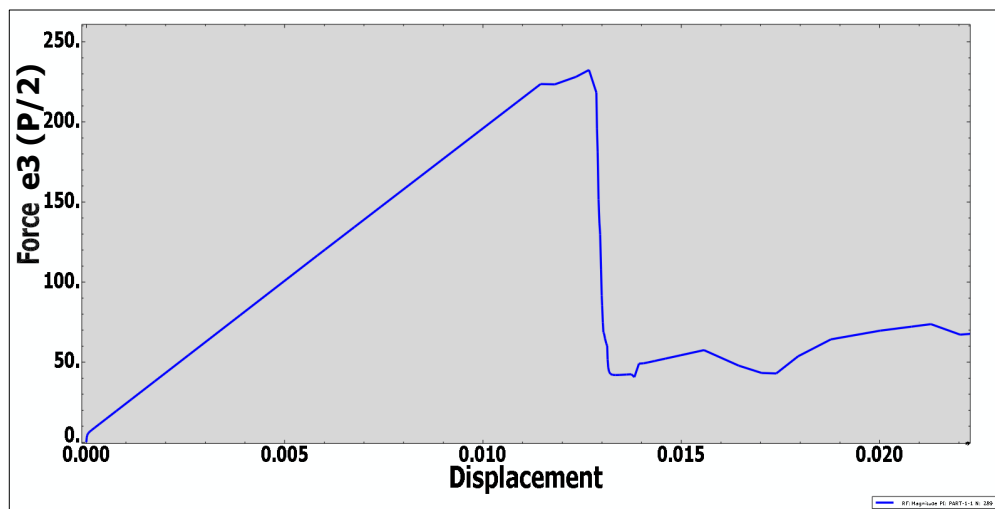


Figure 38: Load-displacement curve of four-point bending beam example



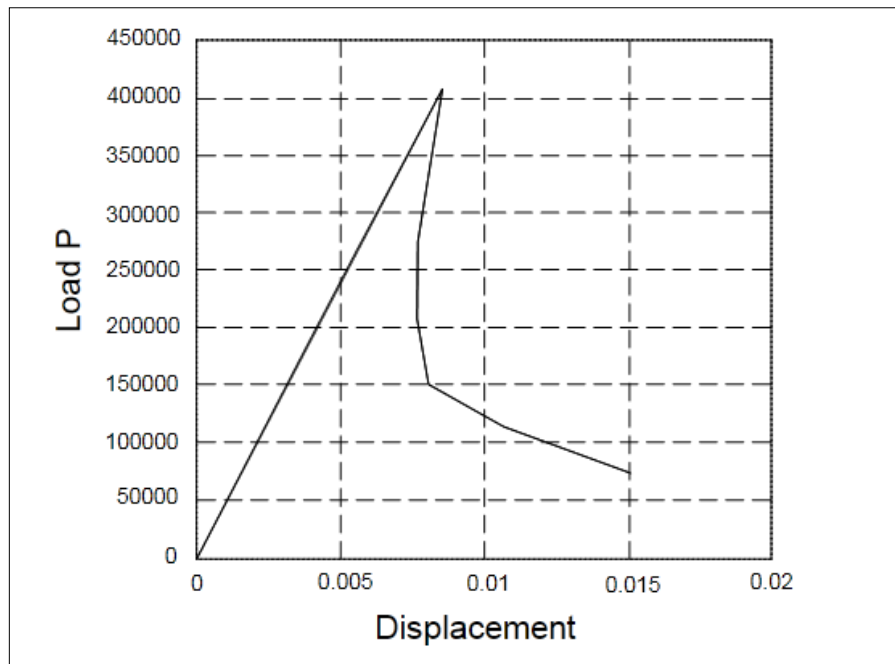


Figure 39: Load-displacement curve of four-point bending beam example from textbook by Mohammadi (Mohammadi 2008)

## **CHAPTER IV**

### **NUMERICAL MODELING AND ANALYSES**

The objective of this thesis study is to provide computational analyses of the differential shrinkage problem encountered on centrifugally-cast concrete members. Details of the problem are explained in Chapter 2; and theoretical background of modeling assumptions is given in Chapter 3.

This chapter consists of the comprehensive description of finite element analyses which are performed with the purpose of revealing the development of stresses induced by the differential shrinkage problem. Following the FEM analyses, the application of the extended finite element method for crack propagation simulations will be explained in this chapter as well. Two and three-dimensional mathematical models are constructed by using ABAQUS (version 6.10). ABAQUS is a powerful commercial finite element analysis tool; which is also capable of solving fracture problems by means of several techniques including the XFEM.

In Chapter 3, it was emphasized that the use of cohesive crack modeling is the proper method of solving concrete fracture problems. Cohesive cracking can be applied through the XFEM formulation by assigning the corresponding material properties in ABAQUS. The details of fracture modeling will be described thoroughly.

#### **4.1 Two-Dimensional Analyses**

As it was stated before, this study is based on the findings of the experimental studies on damaged concrete poles. The details of experimental studies are presented in Chapter 2, along with the information about centrifugal-casting technique, and the differential shrinkage problem due to segregation. Two-dimensional analyses are implemented so as to represent the problem by using the same material properties and conditions in the experiments.

#### 4.1.1 Plane-Strain Assumption

The first stage of the study is the construction of two-dimensional models. To this end, the subject case is simplified to a plane elasticity problem by the plane-strain assumption. As mentioned before, the plane-strain assumption is valid for the members whose third dimension is much larger than the other two dimensions; and also for the loads that do not have components in that dimension. Under that circumstance, the displacement component in the larger dimension becomes so small that it can be neglected in the calculations. The corresponding stress-strain relations are given in Equation (5). Two-dimensional solution of pole structures can be achieved by using the plane-strain assumption and neglecting the displacements and strains through the pole length (Figure 40).

In conjunction with the plane-strain assumption, the CPE4R (4-node bilinear plane strain quadrilateral) element type of ABAQUS is assigned to the member for the finite element analysis (Figure 41).

#### 4.1.2 Model Geometry

The finite element models are prepared in accordance with the geometry and dimensions of specimens presented in the experimental studies (Dilger, Ghali and Rao 1996). In this way, the results of analyses can be compared with the experimental data. The overall dimensions of the pole specimens are shown in Figure 40 of Chapter 2. In compliance with these dimensions, a cross-section with 350 mm outer diameter and 60 mm wall thickness is specified for the two-dimensional analyses as shown in Figure 42a. The member is discretized into approximately 28000 quadrilateral elements. The edge length of the elements is determined as 2 mm, so the cross-section thickness is divided into 30 layers (Figure 42).

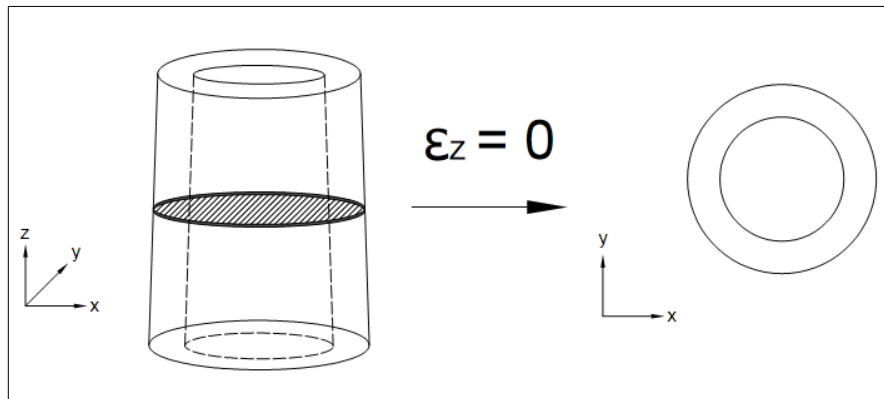


Figure 40: Plane-strain assumption for two-dimensional pole models

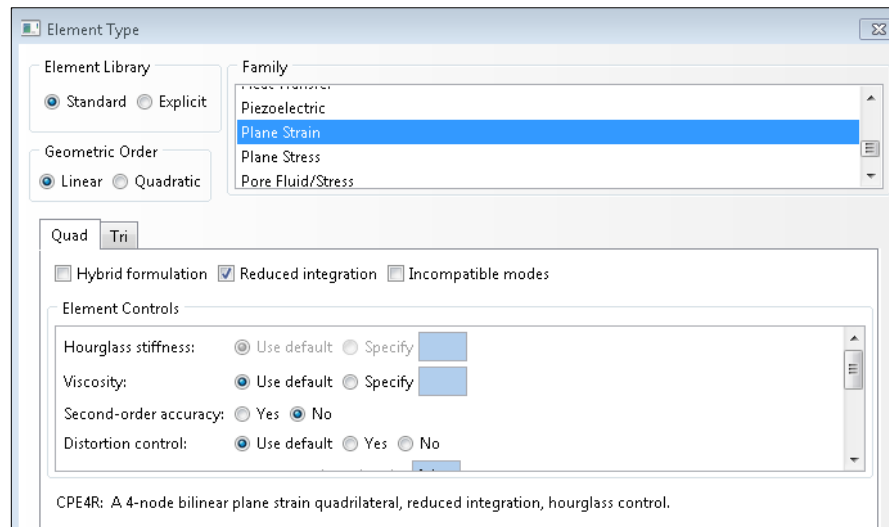


Figure 41: Selection of the element type in ABAQUS

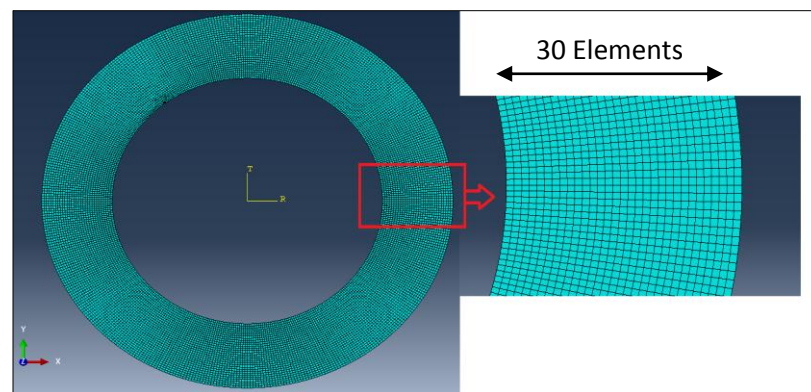


Figure 42: Discretization of the member

#### 4.1.3 Designation of the Boundary Conditions

Analyses are performed with the purpose of revealing the stress growth induced by differential shrinkage. Therefore, the primary consideration while setting the displacement boundary conditions is to avoid development of additional stress concentrations due to improper restraining. To that end, the displacement restraints are arranged in a way that only the rotation of the member is prevented, while its radial expansion in two directions are allowed (Figure 43). In this case, no stress would generate when the member is subjected to uniform shrinkage strains instead of differential shrinkage strains.

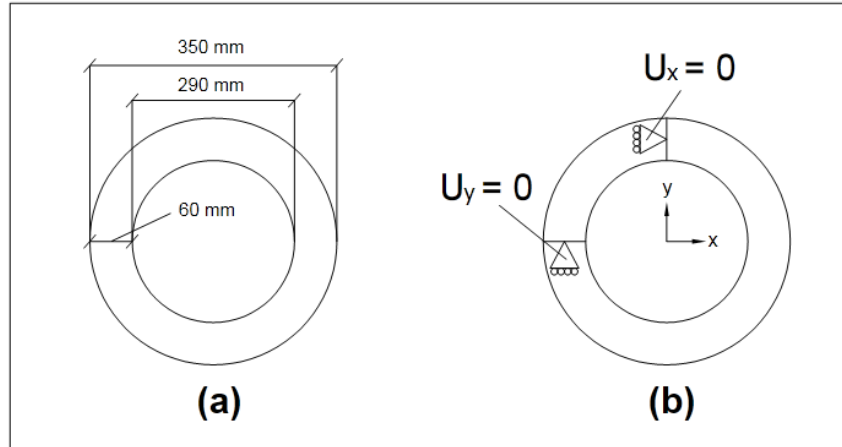


Figure 43: (a) 2D model dimensions, (b) Boundary conditions

#### 4.1.4 Material Properties

##### 4.1.4.1 Implementation of Differential Shrinkage

As mentioned in the second chapter, non-uniform circumferential strains may be generated in inner and outer layers of the spun-cast concrete pole section, when the production method has not been applied properly and cause segregation. In order to investigate this specific problem, the differential amount of shrinkage needs to be assigned throughout the cross-section of the member.

The nonlinear distribution of shrinkage over the section was introduced in Figure 11. Therefore, a parabolic shrinkage distribution is used in the analyses. According to the experimental data (Dilger and Rao 1997), the amount of shrinkage measured in the outermost layer of pole specimens is ten times less than the innermost layer (Figure 44).

To assign the described distribution to the member, an “*analytical field*” is defined in ABAQUS. Analytical fields are used to assign varying properties to members with respect to a selected coordinate system. A cylindrical coordinate system, origin of which is located in the center of member, is created. Next, the varying distribution of shrinkage is defined by means of an analytical field connected to this coordinate system. After defining the distribution profile, shrinkage strain of the outermost layer,  $-250\text{e-}6$ , is assigned to the material as the coefficient of expansion to the material. This value increases by ten times in the innermost layer of the cross-section by means of the analytical field definition.

#### 4.1.4.2 Elastic Properties

The elastic material properties are specified assuming that the concrete mixture have an average characteristic compressive strength of 30 MPa. The corresponding values are depicted in Table 3.

Table 3: Elastic material properties

E (Young's Modulus)	26480 MPa
$\nu$ (Poisson Ratio)	0.2

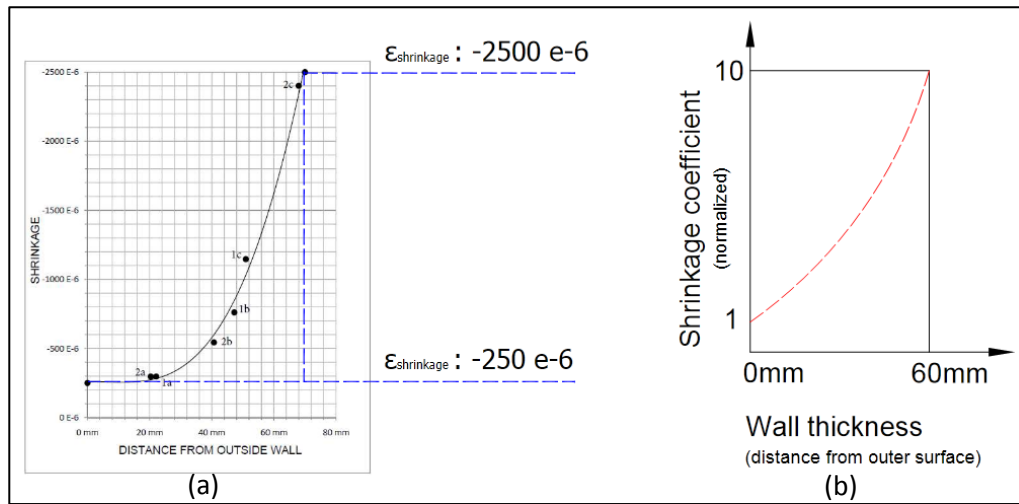


Figure 44: (a) Nonlinear distribution of experimental shrinkage measurements (Dilger and Rao 1997), (b) Parabolic shrinkage distribution curve

#### 4.1.4.3 Other Material Properties

The density and the specific heat properties, which are necessary for the fulfillment of the analysis, are also assigned to the material. The values of  $2400 \text{ kg/m}^3$  and  $1 \text{ e-6 joule/kg} \cdot \text{C}^\circ$  are used for these parameters respectively; they have no significance to the results though. The fracture parameters will be explained in the subsequent parts.

#### 4.1.5 Loading Conditions

Shrinkage of concrete is defined as the coefficient of expansion which is a function of temperature change. In this problem, the change of temperature stands for the change of

time; therefore a unit temperature change is introduced to the member to represent the required amount of time to reach the maximum shrinkage strain.

The relation between time and shrinkage is depicted in Equation (34); where  $\epsilon_r$  is the shrinkage strain,  $\alpha_s$  is the shrinkage coefficient and  $\Delta_t$  is the change in time. Time is defined by means of "predefined fields" of ABAQUS. Two predefined fields are created; first one is for the initial condition and equals to zero, the second one equals to the unit time change. The abovementioned analytical field is used with the second predefined field to realize the differential shrinkage.

$$-\epsilon_r = -\alpha_s \times \Delta_t \quad (34)$$

## 4.2 Two-Dimensional Stress Analyses Results

The obtained results of two-dimensional plane elasticity models will be introduced in this part. It is aimed to show the relation between differential shrinkage and tensile stress development.

### 4.2.1 Development of Stresses

Development of tensile stresses is observed by gradually increasing the intensity of differential shrinkage distribution. In that way, the significance of segregation and its effect could be better seen.

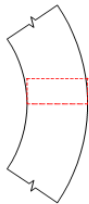
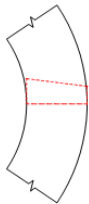
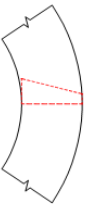
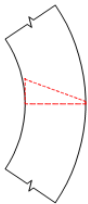

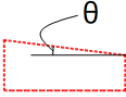
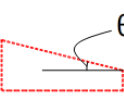
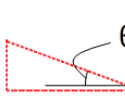
CASE 1		CASE 2		CASE 3		CASE 4	
							
inner $\epsilon$ -2500e-6	outer $\epsilon$ -2500e-6	inner $\epsilon$ -2500e-6	outer $\epsilon$ -1750e-6	inner $\epsilon$ -2500e-6	outer $\epsilon$ -1000e-6	inner $\epsilon$ -2500e-6	outer $\epsilon$ -250e-6
							

Figure 45: Analyses cases with increasing shrinkage gradient

In the first case, the inner and outer shrinkage strains are kept equal to each other. The maximum shrinkage strain,  $-2500e-6$ , is assigned to the whole section. The amount of shrinkage remains the same in the inner layer in the following cases; however, it is decreased linearly through the outer layer. The stages of increasing shrinkage distribution are illustrated in Figure 45. The outermost layer's shrinkage value is decreased by three-tenths of the maximum shrinkage at the each case; and so, in the fourth case, the maximum shrinkage gradient is obtained. The results of these analyses cases are given in the subsequent parts.

#### 4.2.1.1 Results of the First Case

The maximum principal stress diagrams of the first case are given in Figure 46. The results indicate that a uniform shrinkage distribution does not cause any in-plane principal stress concentration, even with the maximum shrinkage strain assigned to the whole section. Therefore no cracking is expected, if the spun-cast concrete has not segregated during production.

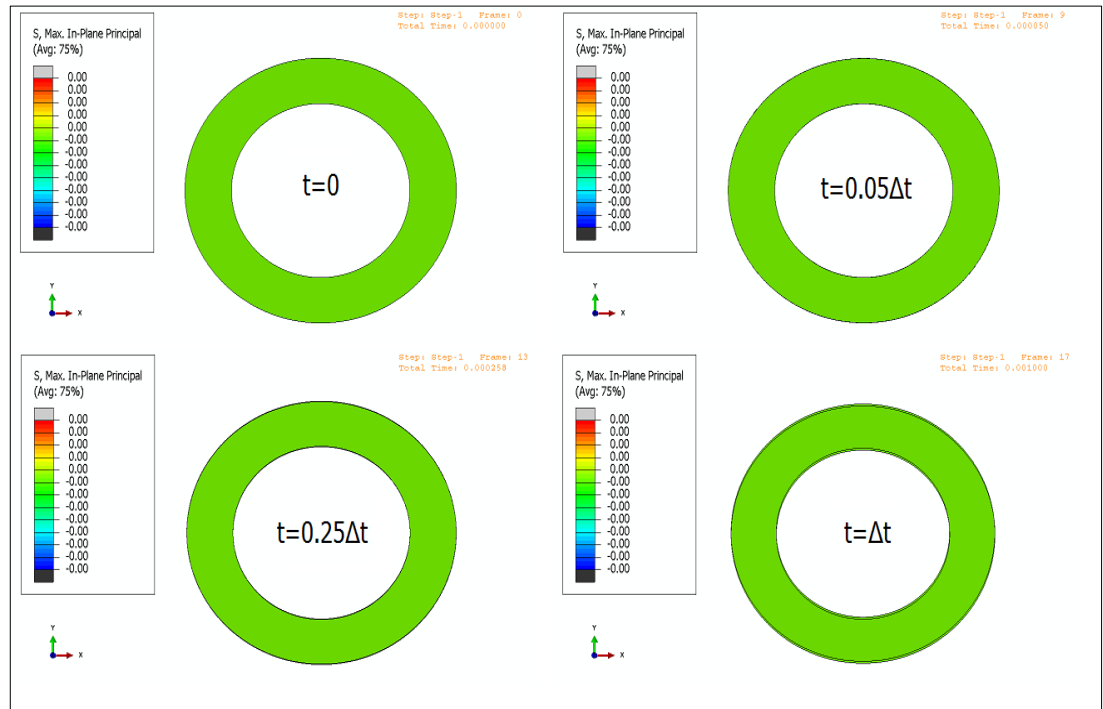


Figure 46: Maximum in-plane principal stress diagrams – Case 1



#### 4.2.1.2 Results of the Second Case

The influence of the differential shrinkage can be seen in the maximum in-plane principal diagrams of the second case (Figure 47). The generated stresses are depicted at four distinct stages of the total analysis duration. The gray colored contour is used to indicate the stresses which exceed the tensile strength of concrete (calculation of concrete tensile strength is given in Section 4.3.1), thus the initiation of cracking can be traced. According to the diagrams, the initiation of cracking is expected to occur at one-fourth ( $0.25\Delta t$ ) of the total duration,  $\Delta t$ .

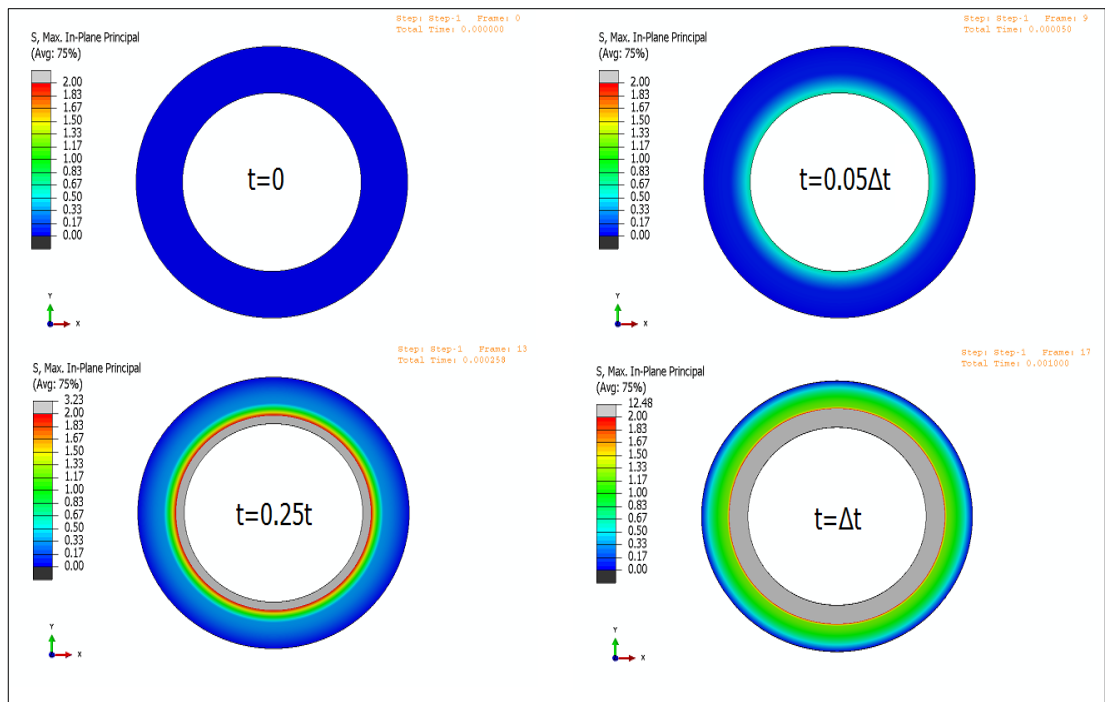


Figure 47: Maximum in-plane principal stress diagrams – Case 2

#### 4.2.1.3 Results of the Third Case

With the further increased shrinkage gradient, effect of the tensile stresses become more significant, and reach to the cracking level earlier (cracking start at  $0.11\Delta t$ ) than the second case (Figure 48). Furthermore, it can be seen that the extent of the expected cracking zone is larger at the end of analysis. Cracking zone spreads beyond the half of cross-section thickness.

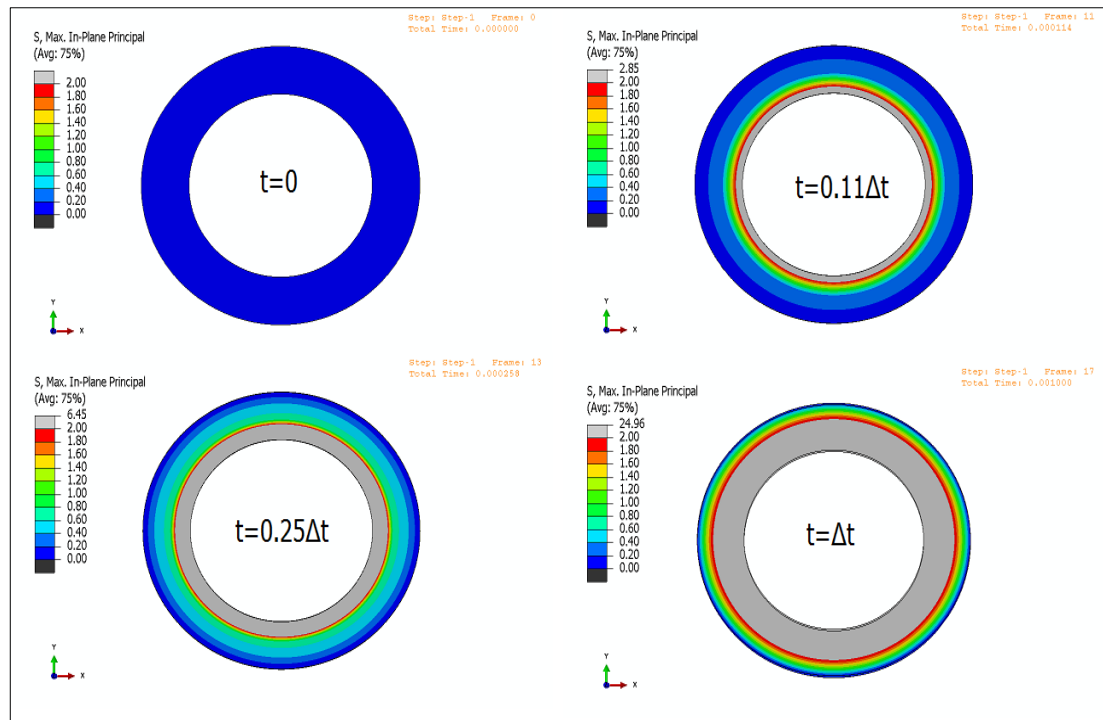


Figure 48: Maximum in-Plane principal stress diagrams – Case 3

#### 4.2.1.4 Results of the Fourth Case

The last case of analyses is performed based on the shrinkage measurements of experimental studies; and represents the steepest shrinkage difference throughout the cross-section. It can be observed from Figure 49 that the cracking initiates at  $0.08 \Delta t$ ; and the cracking zone spreads almost over the whole member.

#### 4.2.2 Interpretation of the Analyses Results

The reason of longitudinal cracking problem observed in spun-cast concrete poles has revealed by experimental studies in literature. Based on the data provided by these studies, two-dimensional analyses of the pole cross-section are performed within this study. The analyses have pointed out the distribution and development of stresses induced by differential shrinkage, throughout the cross-section of poles. The higher shrinkage tendency leads to concentration of tensile stresses in inner layers of poles, which is accordant with the results presented by studies in the literature.

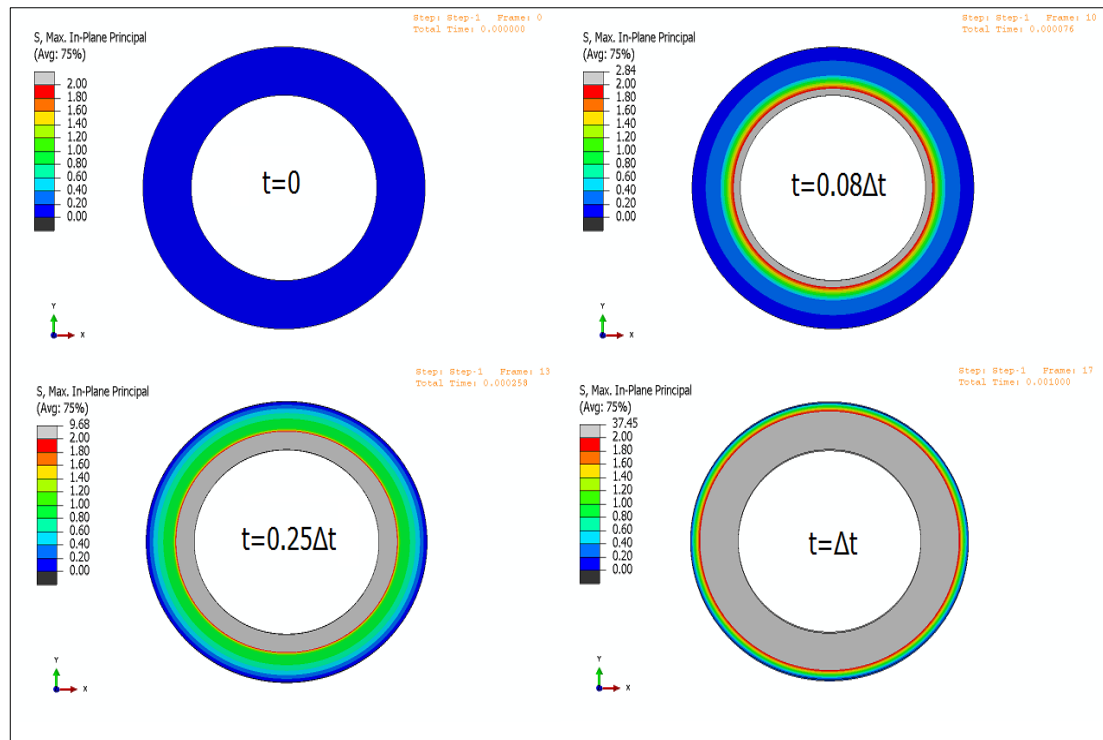


Figure 49: Maximum in-plane principal stress diagrams – Case 4

With the intention of providing a comparative view of stress development, analyses are performed in four cases by changing the intensity of shrinkage difference between the layers of pole cross-section. The analyses results are summarized in Table 4.

Table 4: Summary of the results

Analysis Case	Shrinkage Gradient ( $\tan\theta$ )	Maximum Shrinkage ( $-\epsilon_r$ )	Initiation of Cracking	Extent of Cracking Zone
1	0	-2500e-6	No Cracking	No Cracking
2	$1/3 \theta$	-2500e-6	$0.25\Delta t$	$\approx 1/2$ Thickness
3	$2/3 \theta$	-2500e-6	$0.11\Delta t$	$\approx 3/4$ Thickness
4	$\theta$ experiment	-2500e-6	$0.08\Delta t$	$\approx$ Whole Section

Table 4 shows that the last case, which is performed based on the experimental measurements, exceeds a critical level of shrinkage gradient; and the excessive tensile

stresses develop over the whole section. In this case, it is expected that crack propagation will reach to the outer surface of the pole and lead to durability problems.

### **4.3 Two-Dimensional Crack Propagation Analysis**

The extended finite element method (XFEM) for crack propagation analysis is introduced in Chapter 3. Briefly, XFEM can be used to model discontinuities by means of enriched shape functions and it removes the necessity of remeshing techniques for crack propagation. XFEM is available in ABAQUS; and it can be used by setting parameters in the interaction module.

#### **4.3.1 Crack Initiation Criterion**

Crack initiation can be considered on the instant where the material reaches to the peak point of the load-deformation response. After that point, material begins to undergo a softening behavior and lose its stiffness gradually. The initiation criteria can be defined by several ways such as the maximum principal stress (or strain), maximum nominal stress (or strain) and the quadratic traction (or separation) interaction. In this study, the maximum principal stress criterion is used. It assumes that the cracking initiates when maximum principal stress becomes equal to the specified value; however, a pure compressive state of stress does not cause cracking (ABAQUS 6.10 2010).

The cracking strength is assumed to be equal to the tensile strength of concrete. It is calculated with Equation (35) (Turkish Standards Institution 2000). According to this equation, for a concrete class that have 30 MPa of characteristic compressive strength will have a 1.92 MPa characteristic strength.

$$f_{ctk} = 0.35 \times \sqrt{f_{ck}} \quad (35)$$

In ABAQUS, the damage initiation criterion can be defined by using the material editor in the property module. From the mechanical properties the “damage for traction separation laws” is set to “Maxps Damage” as shown in Figure 50.

#### **4.3.2 Crack Propagation Criterion**

In Chapter 3, the concept of cohesive crack modeling is introduced. It is an established approach to represent the fracture characteristics of concrete. It is also mentioned that cohesive crack models can be successfully achieved by using XFEM. In ABAQUS models, the tension softening behavior of concrete can be implemented by specifying the maximum crack opening displacement or the fracture energy. In this study, the fracture energy is specified for crack propagation.

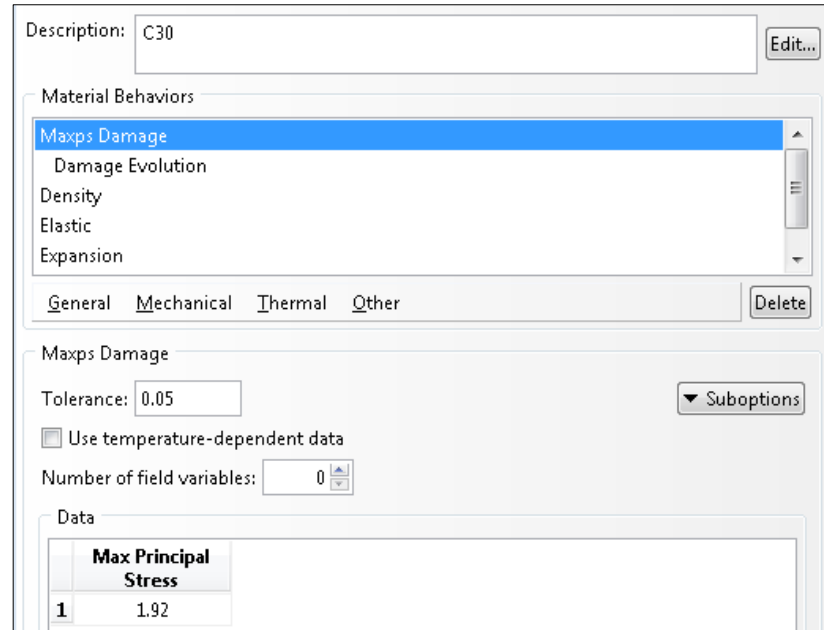


Figure 50: Setting the damage initiation criterion

#### 4.3.2.1 Calculation of the Fracture Energy

The method of calculating fracture energy is described in the Section 3.1.2.2, Equation (27). Simply, the area enclosed with the softening curve is equal to the fracture energy (Figure 51). To calculate the area, there are two required unknowns; first one is the tensile strength of the material; and the second one is the critical crack opening displacement. As it is explained in Section 3.1.2.2, the critical crack opening displacement means that material loses its capability to transfer loads across the crack surface when it reaches to that displacement. This displacement value can be taken as 0.16 mm according to experimental studies in the literature (Shi, Crack Analysis in Structural Concrete 2009). The tensile strength is taken to be 1.92 MPa. Accordingly, the fracture energy is calculated as (for concrete having 30 MPa of characteristic compressive strength):

$$G_f = 1.92 \times 0.16 \times 0.50 = 0.15 \text{ N/mm} \quad (36)$$

ABAQUS enables the definition of both linear and nonlinear softening curves. In this study, the softening curve is taken as linear. The properties of crack propagation are defined by using the "damage evolution" option inside the material editor as shown in Figure 52.

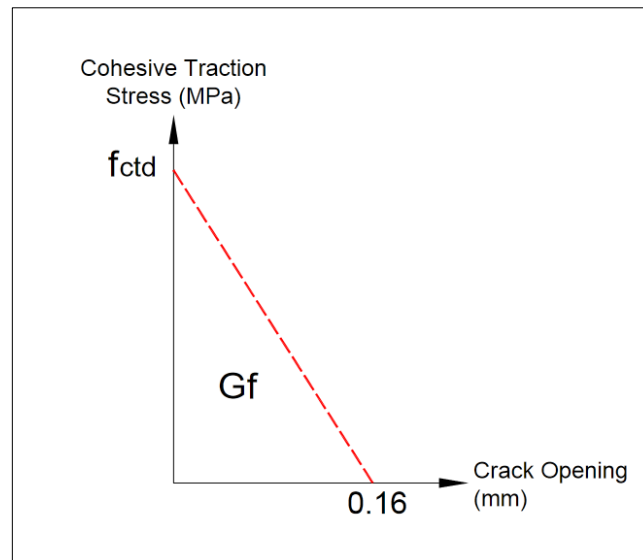


Figure 51: The softening curve of concrete

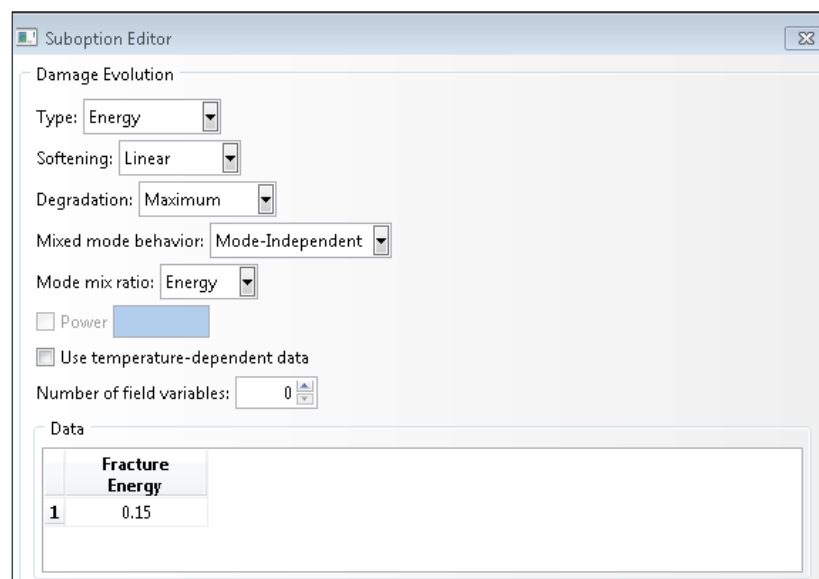


Figure 52: Setting the crack propagation criterion

#### 4.3.2.2 Location of the Crack Initiation

Without any imperfections cracking can start concurrently from more than one point where the stresses reach the specified value. However, in real life there are defects within a material. The tensile strength of these points is lower than the average; therefore, it is

statistically expected that cracking will start from one of these points. Especially, in concrete-like materials, which have an inhomogeneous structure, imperfect points become significant for a crack initiation. Thus, a distinct material, which has the half of the specified tensile strength and half of the fracture energy, is assigned to a small region to ensure that cracking initiates from a single point (Figure 53).

#### 4.4 Results of the Two-Dimensional Crack Propagation Analysis

The same two-dimensional analysis which is described in the preceding section (Step 4: based on the experimental data) is performed for crack propagation. The same model with the same material properties and boundary conditions is used; but this time, the calculated crack initiation and propagation criteria are incorporated. By using the interaction module of ABAQUS, an interaction is defined to enable the XFEM crack growth within the analysis.

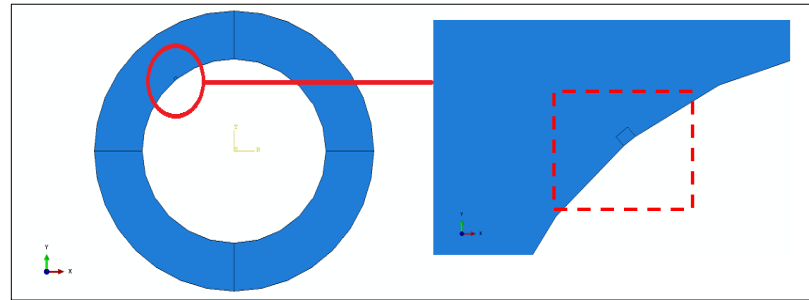


Figure 53: Imperfection for the crack initiation

The result diagrams of the crack propagation stages are shown in Figure 54. As intended, a single crack initiates from the point, where less strength and fracture energy values are assigned for representing an imperfection. The initiation of cracking was estimated to happen at 0.08 of the total duration in the stress analysis. The diagrams show that cracking begins earlier than this estimation ( $0.004 \Delta t$ ). The reason of earlier cracking is the lower strength of defected point.

As it can be seen from the diagrams, the crack has propagated through the whole cross-section, and almost reached to the outer surface. In that case, the cracked pole surface becomes prone to environmental effects. Therefore, this result confirms that the longitudinal cracking, which initiates from the inner surface of poles, can lead to serious durability problems.

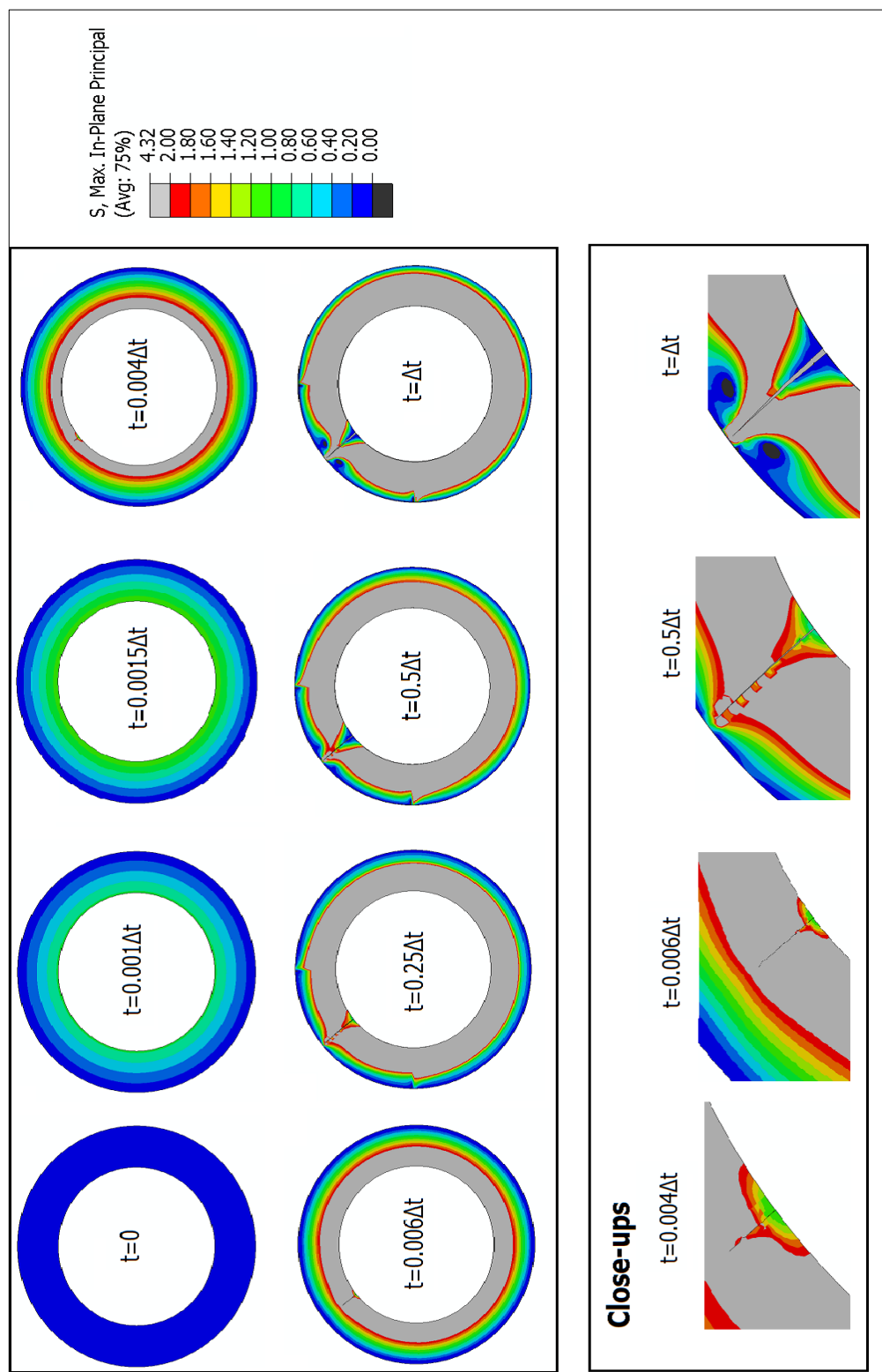


Figure 54: Stages of the crack propagation



## 4.5 Multiple Crack Formation

In Figure 12, it is seen that multiple cracks have initiated in the inner surface of the laboratory specimen. Thus, simultaneous formation of cracking due to differential shrinkage is possible, so it should be considered. To that end, the same two-dimensional analysis is performed by removing the imperfect zone. The obtained crack pattern and stress distribution is shown in Figure 55.

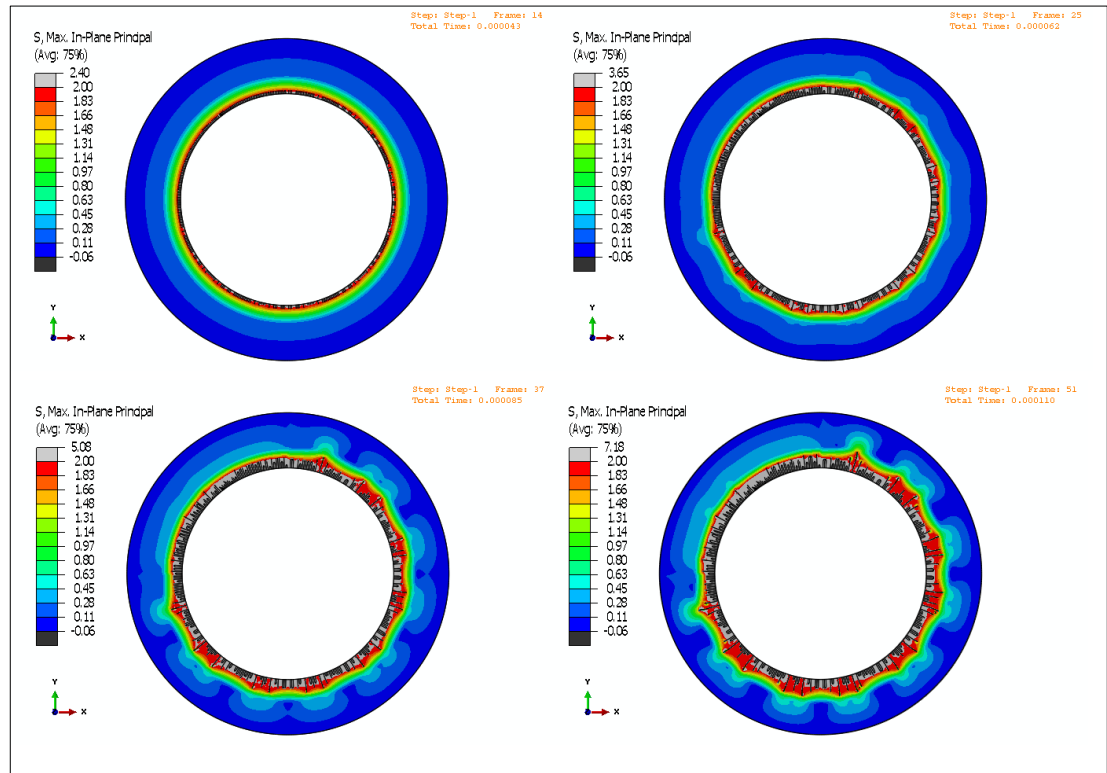


Figure 55: Simultaneous multiple crack formation

The results have shown that cracking can start without an imperfect zone is described. In that case, all cracks initiate simultaneously when the in-plane principal stress exceeds the tensile strength of the concrete. The crack spacing of the obtained pattern is significantly smaller than the actual case. The assigned fracture energy is examined parametrically with the intent of having more realistic crack spacing; however it has been understood that fracture energy parameter is not effective on crack spacing. Consequently, this solution only indicates the prospect of multiple crack formation.

#### 4.6 Effect of Reinforcement

In the experimental studies, it is reported for the reinforced specimens that the crack propagation is usually terminated by a longitudinal rebar which is located near the crack path. In order to investigate this case, the two-dimensional model is modified by incorporating a reinforced zone near the crack initiation point (Figure 56a). For accounting the weak zone between reinforcement and concrete, a smaller modulus of elasticity ( $10^3\text{MPa}$ ) is assigned to the reinforced zone.

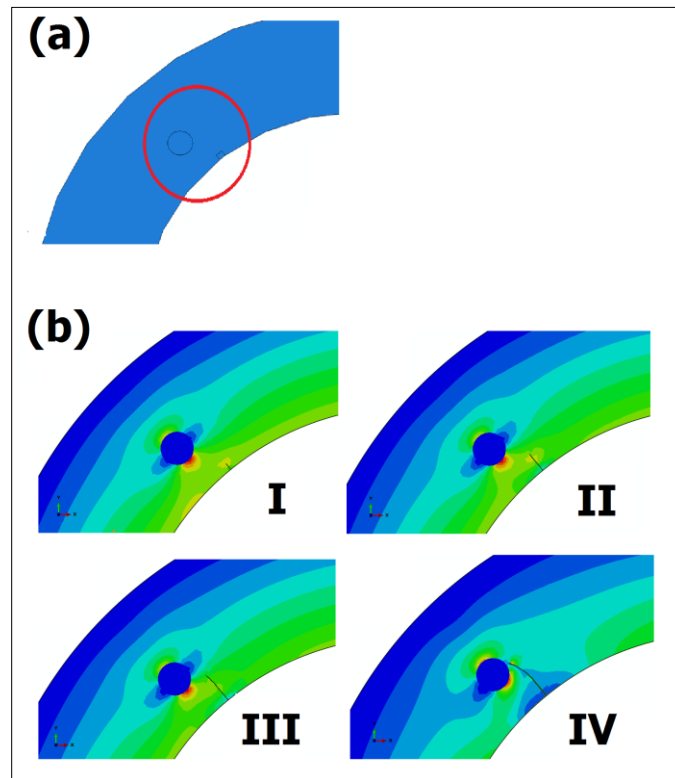


Figure 56: Crack propagation in reinforced cross-section

Four steps of the crack propagation in reinforced cross-section are presented in Figure 51b. In the third step, direction of the crack path steers towards the rebar as the crack-tip approaches to the reinforced zone. Eventually in the fourth step, crack-tip reaches the rebar and the crack propagation stops. This result is in line with the experimental observations, and it confirms that crack propagation terminates if there is a rebar in the vicinity of the crack path.

## 4.7 Three-Dimensional Analyses

After the problem has been investigated with two-dimensional finite element analyses, three-dimensional finite element models are also constructed. The purpose is to compare two and three-dimensional solutions in order to check the consistency of the obtained results.

### 4.7.1 Model Geometry and Properties

The three-dimensional analysis model is constructed by extruding the two-dimensional cross-section by 500 mm in the third dimension. Even though the actual lengths of the poles are much longer, modeling the full length will be computationally impractical. Therefore, a 500 mm thick section of a concrete pole is modeled. It can be observed in Figure 4 that the investigated poles have a narrowing profile through their length. That means the poles' cross-section diameter is larger at the bottom. However, this geometrical property of poles is neglected in the three-dimensional analyses, and the model is constructed with a constant diameter.

Boundary conditions, material properties, fracture parameters and the loading conditions remain the same with the two-dimensional models. Besides the three-dimensional geometry, the only difference between the two models is the element type used. C3D4 (4-node linear tetrahedron) element type of ABAQUS is used for the analysis, and the domain is discretized into 557804 elements (Figure 57).

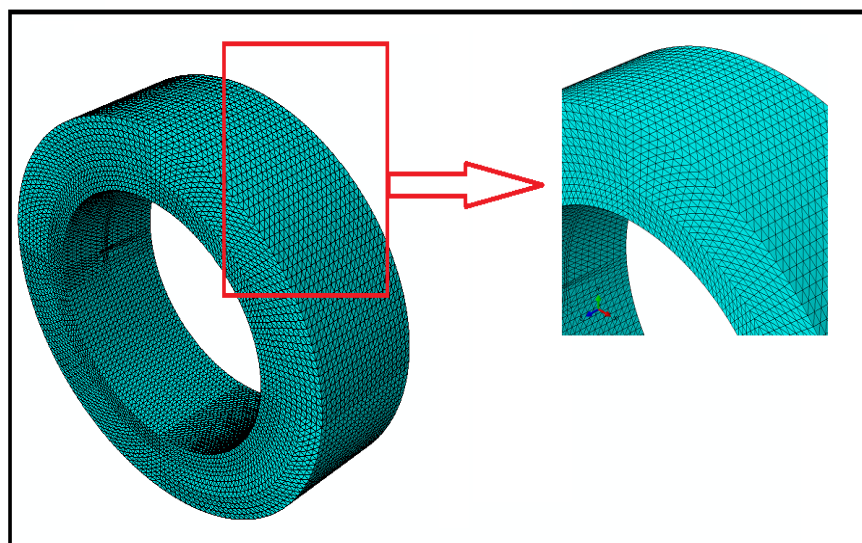


Figure 57: Three-dimensional analysis model

#### 4.8 Results of the Three-Dimensional Stress Analysis

Two cases of three-dimensional stress analyses are performed by implementing the uniform shrinkage in the first case and the most severe differential shrinkage in the second case. The first case is performed to show that a uniform shrinkage distribution does not lead to any stress development through the pole section. The results are depicted in Figure 58, and verify that the shrinkage deformations take place without any stresses generated.

The most severe differential shrinkage is assigned to the section in the second case; therefore, the obtained results are comparable to the fourth case of the two-dimensional analyses. The analysis results of the second case are shown in Figure 59. Similar to the two-dimensional analyses results, the grey colored contour is used to spot the cracking zone. The cracking is expected to start at  $0.09\Delta t$ , which is very similar to the results obtained in the fourth case of the two-dimensional analyses. Furthermore, the extent of cracking zone is also similar; and, it is spread over the whole section. Under that circumstance, crack propagation is expected to reach to the outer surface.

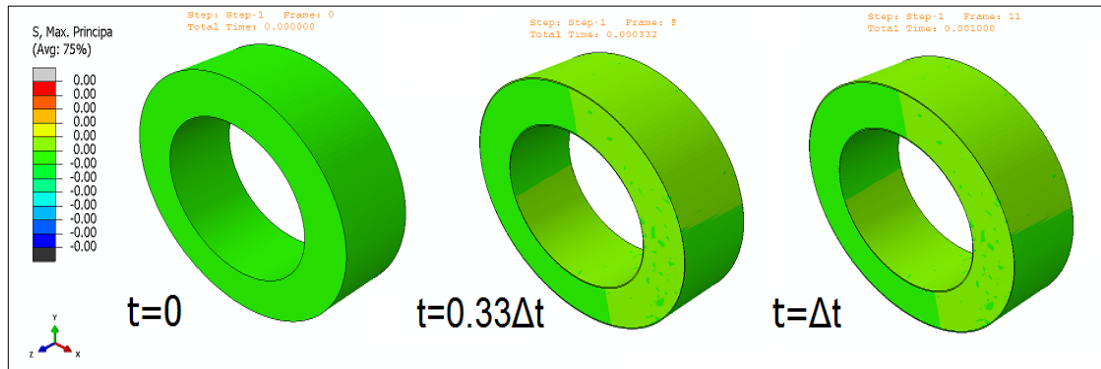


Figure 58: Maximum principal stress diagrams – Case 1

#### 4.9 Results of the Three-Dimensional Crack Propagation Analysis

A crack propagation analysis is performed for the three-dimensional problem. In parallel with the two-dimensional case, three-dimensional model is also constructed by incorporating the fracture parameters of concrete into the stress analysis model. An imperfect region, which is a cubic part located at mid-height of the member, is formed on the inner surface by assigning lower strength and fracture energy criteria in order to obtain a single crack initiation.

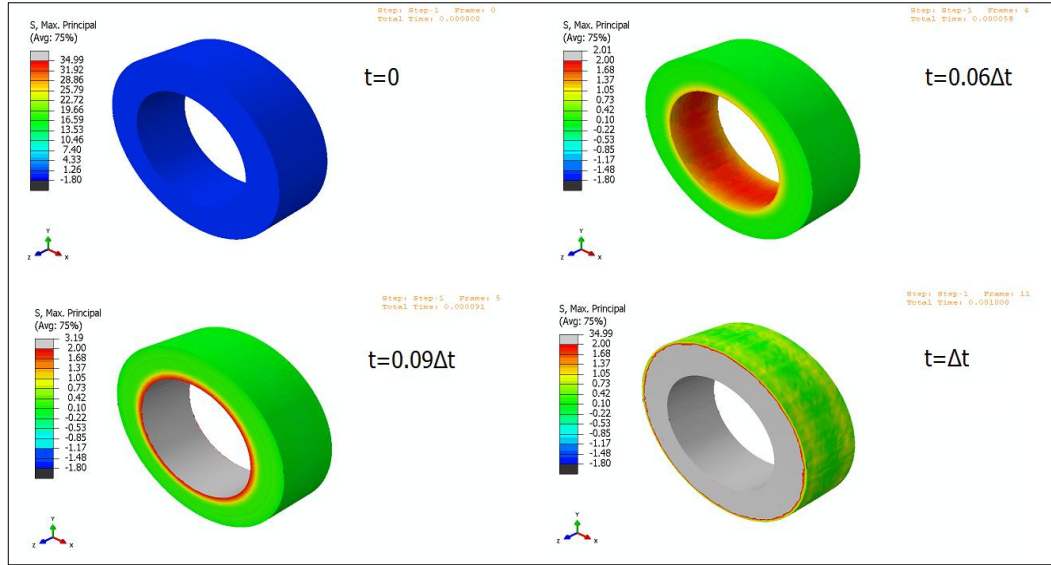


Figure 59: Maximum principal stress diagrams – Case 2

The obtained results are presented in Figure 60 in terms of the level set contours. It can be seen that the crack initiates from the defected point on the inner surface of the pole. The initiation of cracking occurs at  $0.02\Delta t$ . Cracking begins earlier than the estimation of stress analysis due to the lower strength of imperfect zone. The initiated crack propagates in two directions; the first direction is towards the outer surface and the second is along the longitudinal dimension of pole. The three-dimensional crack surface is formed with combination of propagation in these two directions; therefore, the complete longitudinal crack geometry is obtained.

#### 4.10 Discussion on Limitations of the Study

In this study, a time-dependent behavior of concrete and its effects on structural elements is investigated. However, in the computational analyses the elastic properties of concrete, which are also dependent on time, are considered to be constant for sake of simplicity. In this case, the early-age tensile strength and modulus of elasticity of concrete are overestimated. If these parameters were regarded as time-dependent parameters, then an earlier crack initiation would be obtained in fracture analyses.

Another modeling assumption is the absence of lateral reinforcement. The plain concrete material properties are assigned to the pole sections. As a matter of fact, usually spiral or hoop steel is incorporated as lateral reinforcement against longitudinal cracking. This study does not account for any lateral reinforcement, so considers the insufficiently reinforced members.

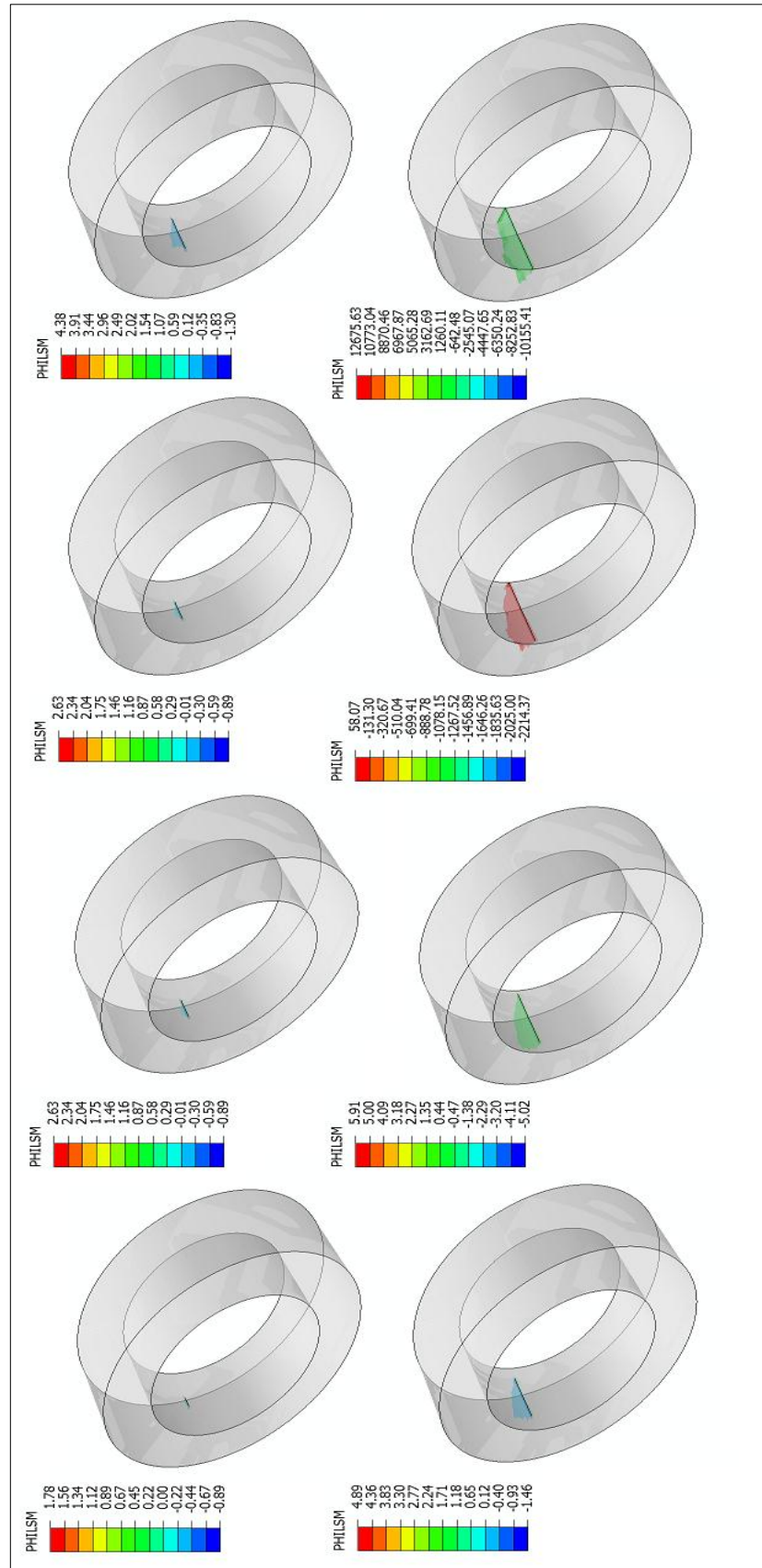


Figure 60: Level set contours of three-dimensional crack propagation

## **CHAPTER V**

### **CONCLUSION AND RECOMMENDATIONS**

Experimental studies of several researchers have revealed the cause of longitudinal cracking problem encountered on spun-cast concrete poles. As per these studies, uneven shrinkage of the segregated layers in a concrete pole cross-section results in severe durability problems by means of cracking.

Based on the measurements presented in the experimental studies, two and three-dimensional finite element models of segregated concrete pole have been constructed. The obtained results of analyses have verified that the tensile strength of concrete is exceeded in the inner layer of cross-section. It has been observed that the cracking zone extends from the inner layer towards the outer layer as the gradient of the shrinkage increases over the cross-section. A similar stress development is obtained by the three-dimensional analyses as well.

The expected concrete fracture has been also modeled by use of XFEM, and a cracking pattern, complying with experimental findings, is simulated. The analysis has shown that a crack can propagate until it reaches the outer surface of the pole. In addition, effect of reinforcements on crack propagation has been studied by a distinct model. The reinforced model has revealed that crack propagation tends to go toward and terminate at a nearby reinforced zone. This result is also concurrent with the findings of experimental studies.

Consequently, it can be concluded that the use of such computational tools may aid the production process and the durability problems can be avoided by conducting a well-designed production phase, thus eliminating segregation of the concrete. The computational analyses have shown that a uniformly casted concrete pole will not suffer from excessive tensile stress formation by uneven shrinkage.

For the future research, it would be interesting to include the diffusion-deformation interaction into the problem to see its effect on the stress development and cracking. Also, the reinforcement arrangement and the concrete cover thickness could be investigated to reveal how they affect the crack initiation.

In this thesis study, the material properties are assigned as if concrete is homogeneous. A more realistic and comprehensive study can be carried out by examining the mesostructure of concrete through the pole section. By this means, it will become possible to assign mechanical properties of constituents individually. Thus, more accurate crack propagation analyses can be conducted.

The XFEM technique in ABAQUS version 6.10 has been used in this thesis study to investigate a fracture problem. The obtained results have shown that XFEM is a reasonable method to model fracture of concrete. Therefore, this method can be used to study the nonlinear behavior of various structural concrete members.



## REFERENCES

- ABAQUS 6.10. "Abaqus Analysis User's Manual." Dassault Systèmes, 2010.
- ACI Committee 446. *Fracture Mechanics of Concrete: Concepts, Models and Determination of Material Properties*. American Concrete Institute, 1991.
- AFG-EL. *Afghanistan Electric*. 2012. Available from: <http://www.afgel.com/> (cited March 2012).
- Asferg, J. L. "Modeling of Concrete Fracture Applying the eXtended Finite Element Method." Ph.D. Thesis 2006.
- Bazant, Z., P. "Concrete Fracture Models: Testing and Practice." *Engineering Fracture Mechanics*, 2002: 165-205.
- Belytschko T., and T. Black. "Elastic Crack Growth in Finite Elements with Minimal Remeshing." *International Journal for Numerical Methods in Engineering*, 1999: 601-620.
- Dilger, W. H., A. Ghali, and S. V. K. M. Rao. "Improving the Durability and Performance of Spun-Cast Concrete Poles." *PCI Journal*, March/April 1996: 68-90.
- Dilger, W. H., and S. V. K. M. Rao. "High Performance Concrete Mixtures for Spun-Cast Concrete Poles." *PCI Journal*, July/August 1997: 82-96.
- Dolbow J., Moës N., Belytschko T. "Discontinuous Enrichment in Finite Elements with a Partition of Unity Method." *Finite Elements in Analysis and Design*, 2000: 235-260.
- Fam, A. "Development of a Novel Pole Using Spun-Cast Concrete Inside Glass-Fiber-Reinforced Polymer Tubes." *PCI Journal*, May/June 2008: 100-113.
- Kudzys, A., and R. Kliukas. "The Resistance of Compressed Spun Concrete Members Reinforced by High-Strength Steel Bars." *Materials and Structures* 41 (2008): 419-430.
- Mehta, P. K., and P. J. M. Monteiro. *Concrete; Microstructure, Properties, and Materials*. New York: McGraw-Hill, 2006.
- Moës N., Belytschko, T. "Extended Finite Element Method for Cohesive Crack Growth." *Engineering Fracture Mechanics*, 2002: 813-833.
- Mohammadi, S. *Extended Finite Element Method: for Fracture Analysis of Structures*. Blackwell Publishing, 2008.
- NavaChing. 04 24, 2008. <http://www.navaching.com/> (accessed March 2012).
- PCI, (Precast / Prestressed Concrete Institute). "Guide for the Design of Prestressed Concrete Poles." *PCI Journal*, November/December 1997.

- Rodgers, T. E. Jr. "Prestressed Concrete Poles: A State-of-the-Art Report." *PCI Journal*, September/October 1984.
- Shi, Z. *Crack Analysis in Structural Concrete*. Burlington: Elsevier, 2009.
- Stolarska M., Chopp D. L., Moës N., Belytschko T. "Modelling Crack Growth by Level Sets in the Extended Finite Element Method." *International Journal for Numerical Methods In Engineering*, 2001: 943-960.
- Turkish Standards Institution. "TS 500: Requirements for Design and Construction of Reinforced Concrete Structures." 2000.
- Zi G., Belytschko T. "New Crack-Tip Elements for XFEM and Applications to Cohesive Cracks." *International Journal for Numerical Methods in Engineering*, 2003: 2221-2240.